

Abstract

Contents

1	Introduction	5
1.1	Overview	5
1.2	Transitional wall-bounded shear flows	8
1.2.1	Linear Stability Analysis	8
1.2.2	Nonlinear dynamical systems	12
1.2.3	Spatiotemporal transitional flows	14
1.3	Rayleigh-Bénard convection	17
1.4	Rayleigh-Bénard Poiseuille (RBP) flows	22
1.4.1	Thesis Outline	24
2	Numerical Techniques	21
2.1	Method of weighted residuals	21
2.2	The Spectral/hp element methods	24
2.3	Temporal Discretisation	26
2.4	Velocity correction scheme for incompressible Navier Stokes equations	28
2.5	Linear Stability Analysis	30
2.6	Edge Tracking	30
3	Transitional Rayleigh-Bénard Poiseuille flows	31
3.1	Introduction	31
3.1.1	Rayleigh-Bénard Poiseuille (RBP) flows	31
3.1.2	Rayleigh-Bénard convection (RBC)	32
3.1.3	Plane Poiseuille flows (PPF)	32
3.1.4	Objectives and organisation	33
3.2	Problem formulation	33
3.2.1	Governing equations	33
3.2.2	Numerical Methods	34
3.2.3	<i>Ra-Re</i> sweep	35
3.2.4	Linear Stability Analysis	35
3.3	<i>Ra-Re</i> Phase Space	36
3.3.1	Classification	36
3.3.2	Spatiotemporal intermittent rolls	38

3.3.3	Coexistence with turbulent bands	40
3.4	The role of longitudinal rolls	41
3.4.1	The thermally-assisted sustaining process (TASP) in a confined domain	41
3.4.2	Variation of Ra and Re on the thermally sustained turbulent process within $\Gamma = \pi/2$	49
3.4.3	Extending to large domains, $\Gamma = 4\pi$	55
3.5	Conclusions	55
4	The state space structure of Spiral Defect Chaos	57
4.1	Introduction	57
4.1.1	Multiple convection states	57
4.1.2	Spiral defect chaos	58
4.1.3	Scope of this study	58
4.2	Problem formulation	59
4.2.1	Rayleigh-Benard convection (RBC)	59
4.2.2	Numerical method	60
4.2.3	Linear stability analysis of ISRs	60
4.3	Transient SDC and elementary states in minimal domain	61
4.4	Multiplicity of edge states	67
4.5	Unstable ideal straight rolls	71
4.5.1	Pathways leading to ISRs - heteroclinic orbits	75
4.5.2	Pathways leading to elementary states	78
4.5.3	A pathway to SDC in an extended domain $\Gamma = 4\pi$	80
4.6	Concluding remarks	84
7	Conclusions	17
8	Appendices	18

Chapter 1

Introduction

1.1 Overview

Fluid motions driven by buoyancy and frictional forces belongs to broad class of flows known as thermoconvective shear flows. These flows exhibit rich behaviour, and are of interest in both engineering and meteorology applications spanning across a broad range of length scales. At small scales, around $L \sim 1\text{cm}$, the thermoconvection flows are relevant to the cooling of microprocessing chips. In such systems, the fluid acts medium to dissipate heat, experiences shear forces from the confining walls, and buoyancy from heating. One of the major innovation in this industry is in squeezing more transistors onto a single chip, resulting to a doubling of transistors on a single chip roughly every two years, according to Moore's law. However, one of the major limitations on further miniaturisation is the challenge of dissipating the excessive heat generated. Fluids, such as air, water or refrigerant, are often used to transport heat away from the components, thereby preventing overheating [Kennedy and Zebib, 1983, Ray and Srinivasan, 1992]. At intermediate length scales, $L \sim 1\text{m}$, the interaction between buoyancy and frictional forces is important in the fabrication of uniform thin films in chemical vapour deposition (CVD) [Evans and Greif, 1991, Jensen et al., 1991]. The CVD process typically involves a reactive gases carried by inert gases which flows through a channel with a heated substrate. Upon heating, the reactant gases react chemically at substrate and deposits material, forming thin films, such as silicon layers. A key challenge in the CVD process is achieving a uniform deposition and maintaining sharp interfaces between layers. The interactions between shear and buoyancy forces often gives rise to boundary layers and thermoconvective rolls, which can disrupt uniform deposition, affecting film quality. At large scales, $L \sim 1\text{km}$, the thermoconvective shear flows can be observed in the atmosphere such as the cloud streets over the Norwegian Sea. These parallel bands of cumulus clouds can stretch over hundreds of kilometres. They form when relatively warm sea surfaces heat up the colder air blowing from the North [nor]. As the colder air is heated, it rises upwards whilst carrying water vapour. As it reaches a certain altitudes, $L \sim 1 - 10\text{km}$, the water vapour condenses into visible clouds, while the cooler air falls towards the sea. This circulation is organised into parallel rotating parallel columns of air, forming distinct cloud streets.

The common thread among the examples discussed above is the interaction between shear and buoyancy forces driven fluid motion - the central focus of this thesis. By restricting our analysis to these

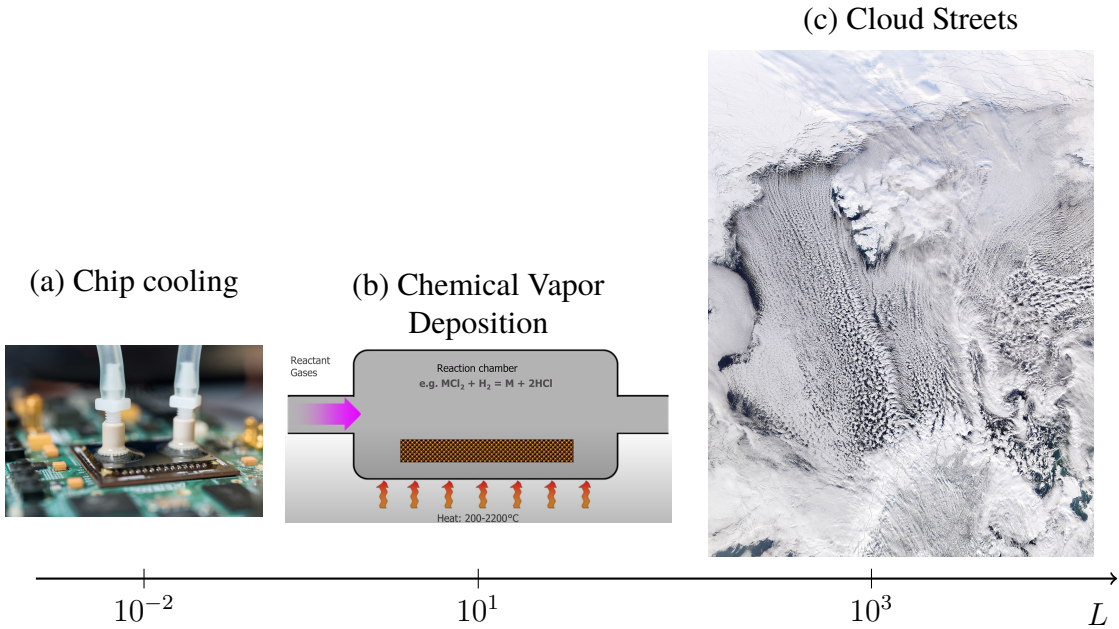


Figure 1.1: Fluid flow due to shear and buoyancy forces across length scales, $L \in [1\text{cm}, 1\text{km}]$, such as (a) chip cooling, (b) chemical vapour deposition and (c) formation of cloud streets.

two mechanisms, we neglect other physical mechanisms such as phase change, chemical reactions and evaporation, which may be significant in the context of cooling microprocessors, chemical vapour deposition, and atmospheric boundary layers respectively [Vallis et al., 2019]. To consider this interaction, we consider an idealised setup without geometric complexity, known to as the Rayleigh-Bénard-Poiseuille (RBP) flow. This system describes the fluid motion confined between two infinitely extended parallel plates, heated from below and cooled from the top, with an additional pressure gradient driving the flow. The RBP configuration combines two paradigmatic flow configurations; the classical Rayleigh-Bénard convection (RBC), driven purely by buoyancy, and plane Poiseuille flow (PPF), driven purely by shear. While the onset of convection in RBC, and the transition to subcritical shear-driven turbulence in PPF have been both extensively studied, the transitional regime in which both forces interact remains less understood. Gaining insights into this regime can have implications for various applications across a range of scales mentioned previously.

The RBP configuration is illustrated in figure 1.1, where $z^*, y^*, x^*, L_z, L_x, d, h$ refer to the streamwise, spanwise, wall-normal coordinates, length, span, depth and half-height of the domain respectively. We note that the asterisks*, refer to variables in dimensional form. The flow is driven by a pressure gradient along the streamwise z^* direction, $\Delta P^* = P^*|_{z^*=0} - P^*|_{z^*=L_z} < 0$, leading to the formation of a laminar Poiseuille flow, $w^*(y^*)$, for a sufficiently small ΔP . In this study, we will only consider fully-developed flow, where the boundary layer from the top and the bottom wall meets at the midplane, $y^* = 0$, and entrance effects are neglected. The RBP configuration is also unstably stratified, such that the temperature difference between the lower, T_L , and upper wall, T_U , is always positive, $\Delta T = T_L - T_U > 0$, leading to a stable linear conduction profile along the wall-normal direction, $T(y^*)$, if ΔT is kept sufficiently small.

In the absence of a pressure gradient, the RBP configuration reduces to the classical Rayleigh-

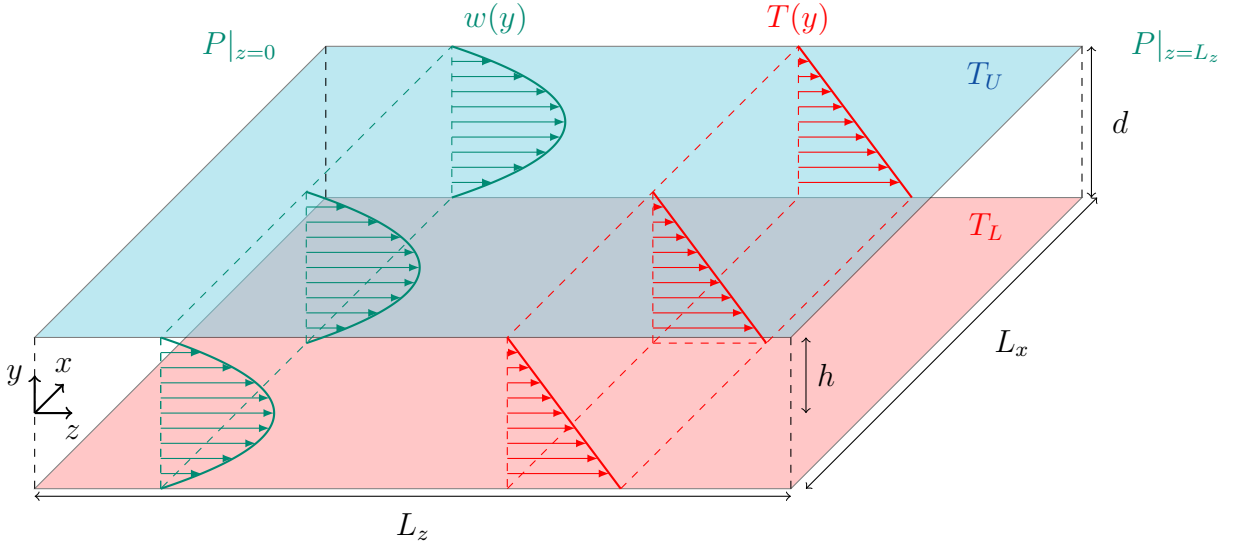


Figure 1.2: The Rayleigh-Bénard Poiseuille (RBP) flow configuration.

Bénard convection problem, bringing about buoyancy-driven convection for a sufficiently large unstable stratification. In the limiting case without unstable stratification, $\Delta T = 0$, the system reduces to the wall-bounded plane Poiseuille flow (PPF), where the transition towards subcritical shear-driven turbulence may be expected for a sufficiently large pressure gradient.

For instance, do buoyancy forces promote the transition to shear-driven turbulence and how does shear influence the convection? To describe the motion of the fluid in RBP configurations, we consider non-dimensionalised Navier-Stokes equations with Boussinesq approximations,

$$\frac{\partial \mathbf{u}}{\partial t} + (\mathbf{u} \cdot \nabla) \mathbf{u} = -\nabla p + \frac{1}{Re} \nabla^2 \mathbf{u} + \frac{Ra}{Re^2 Pr} \theta, \quad (1.1a)$$

$$\frac{\partial \theta}{\partial t} + (\mathbf{u} \cdot \nabla) \theta = \frac{1}{Re Pr} \nabla^2 \theta, \quad (1.1b)$$

$$\nabla \cdot \mathbf{u} = 0. \quad (1.1c)$$

where $\mathbf{u}(\mathbf{x})$, $\theta(\mathbf{x})$, $p(\mathbf{x})$ refers to the nondimensionalised velocity, temperature and pressure respectively. The key control parameters for RBP flows are the Rayleigh number, Ra , Reynolds number, Re , Prandtl number Pr , which are defined as follows,

$$Ra = \eta g d^3 \Delta T / \nu \kappa, \quad Re = W_c h / \nu, \quad Pr = \kappa / \nu, \quad \Gamma = L / 2d, \quad (1.2)$$

where η , g , ΔT , ν , κ , W_c , h , d , L are the thermal expansion coefficient, acceleration due to gravity, temperature difference between the bottom and top wall, kinematic viscosity, thermal diffusivity, laminar centreline velocity, domain's half-depth, full-depth, length or span respectively.

We describe important historical of hydrodynamic stability of planar shear flows and their theoretical frameworks in §1.2. Theoretical frameworks used in the study of stability of flow such as linear stability, nonlinear dynamical systems and spatiotemporal character of transitional shear flows

will be outlined. This followed the historical developments of Rayleigh-Bénard convection (RBC), where concepts of the stability of fluid flows will be utilised in §1.3. After which, we describe the historical developments of RBP flows §1.4, and the outline of the thesis will be give in §1.4.1.

1.2 Transitional wall-bounded shear flows

Wall-bounded shear flows concerns the motion of the fluid flowing in parallel to walls, typically bounded by one or more walls. The fluid closest to the wall comes to a rest, satisfying the no-slip boundary condition in the presence of a wall. As a consequence, a velocity gradient in the direction perpendicular from the wall develops, where the fluid layer becomes *sheared* due to the presence of the wall - referred to wall-bounded sheared flows. Example of wall-bounded shear flows include the pressure-driven plane Poiseuille flow (or channel flow), Hagen-Poiseuille (or pipe) flows, plane Couette flow and flat plate boundary layers. These geometrically simple examples enables a convenient framework amenable to the mathematical analysis of fluid motion subjected to shear. Depending on the degree of shear, the fluid motion can be either laminar, where the fluid layers move in smooth parallel 'laminates', or turbulent, characterised by chaotic eddying motions. We also note that there is a transitional regime where both states can coexist discuss later. A central question is predicting the transition from the laminar regime to the turbulence.

The earliest investigation into this transition dates back to the pipe flow experiments of [Reynolds \[1883\]](#). In his experimental setup, the flow speed through the pipe could be controlled by regulating the inlet pressure, while injecting dye to visualise the flow, as illustrated in figure 1.3(a). At low speeds, the fluid remained laminar, resulting to a single streak of steady dye in figure 1.3(b). As the speed increased, the dye begin to exhibit irregular 'sinuous' motions interspersed with laminar regions shown in figure 1.3(c). This is now referred to as the transitional/intermittent regime, alternating between the laminar and turbulent states. Beyond a critical speed, the dye breaks down entirely into chaotic 'eddies', mixing with the surrounding fluid and discolouring the flow with dye downstream in figure 1.3(d). This regime is now identified as turbulence.

Reynolds conjectured that the threshold between the laminar, transitional and turbulent regimes could be characterised by the Reynolds number, $Re = UD/\nu$, where U is the centerline velocity in the pipe, D , the pipe diameter and ν , the kinematic viscosity. He observed that flow through the pipe remained 'stable' and laminar for $Re < 1900$, while it became 'unstable' and turbulent for $Re > 2000$ [[Reynolds, 1895](#)]. His remarks led to the concept of the stability of fluid flows.

1.2.1 Linear Stability Analysis

Following Reynolds' experiment, interest towards the mathematical analysis of the stability of fluid flows grew in early 20st century. The mathematical approach typically begins by decomposing the velocity field, $\mathbf{u}(\mathbf{x}, t)$, into a laminar (base) state, $U(y)$ (assumed to depend only on the wall-normal direction here), and the velocity perturbations, $\mathbf{u}'(\mathbf{x}, t)$, with pressure similarly decomposed as,

$$\mathbf{u}(\mathbf{x}) = U(y) + \mathbf{u}'(\mathbf{x}, t), \quad \text{and} \quad p(\mathbf{x}, t) = P(x) + p'(\mathbf{x}, t). \quad (1.3)$$

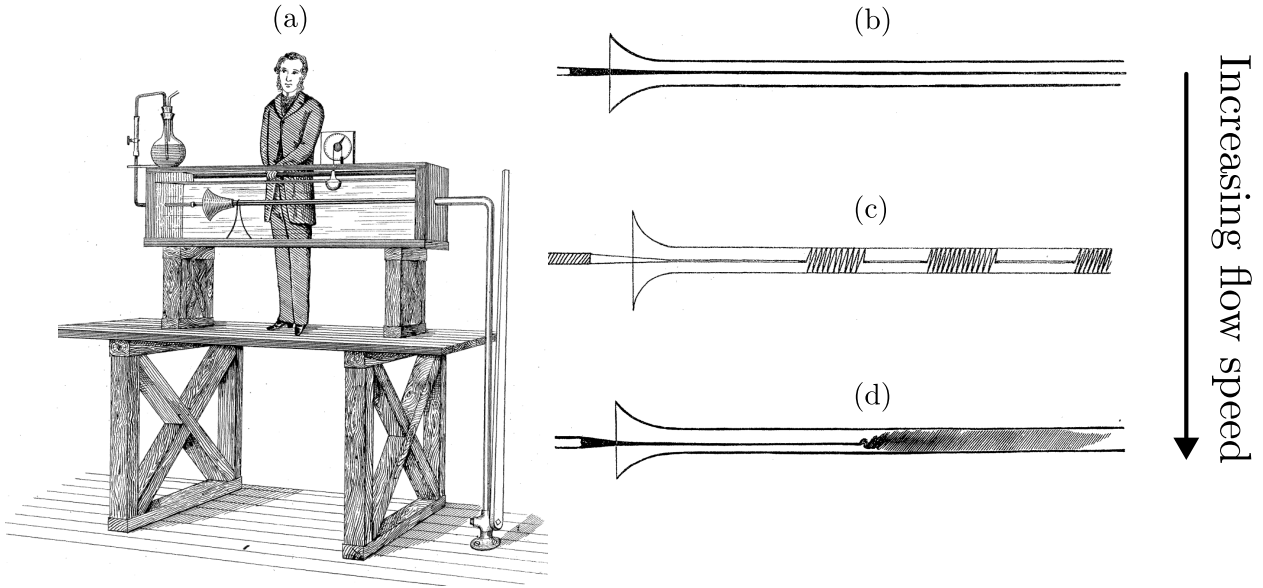


Figure 1.3: (a) Osbourne Reynolds pipe experiment with the dye injection apparatus, illustrating the (b) laminar flow, (c) intermittent regime and (d) turbulent flow as the flow speed is increased, taken from [Reynolds, 1883].

Next, we substitute the formulations for the decomposed velocity and pressure into the Navier-Stokes equations of equation (1.1) and drop the nonlinear perturbations terms $(\mathbf{u}' \cdot \nabla)\mathbf{u}'$,

$$\frac{\partial \mathbf{u}'}{\partial t} + (\mathbf{U} \cdot \nabla) \mathbf{u}' + (\mathbf{u}' \cdot \nabla) \mathbf{U} = -\nabla p' + \frac{1}{Re} \nabla^2 \mathbf{u}', \quad (1.4a)$$

$$\nabla \cdot \mathbf{u}' = 0, \quad (1.4b)$$

resulting to the linearised Navier-Stokes equations. This commonly followed by introducing a wavelike ansatz (mode) defined by streamwise and spanwise wavenumbers, α, β and complex frequency, ω . In general two ways to analyse the linearised Navier-Stokes equations by considering the behaviour of each mode independently in §1.2.1 and their coupled dynamics in §1.2.1

Modal analysis

It is convenient to eliminate the pressure terms by transforming equation (1.4) using the wall-normal perturbation velocity, v' , and wall-normal vorticity, $\eta' = \partial u'/\partial z - \partial w'/\partial x$, variables. Using (v, η) , introduce an ansatz (mode) for them,

$$v'(\mathbf{x}, t) = \tilde{v}(y) e^{i(\alpha x + \beta z - \omega t)}, \quad \text{and} \quad \eta'(\mathbf{x}, t) = \tilde{\eta}(y) e^{i(\alpha x + \beta z - \omega t)}. \quad (1.5)$$

where α, β, ω denotes the streamwise and spanwise wavenumbers, and complex frequency (i.e. $\omega = \omega_r + i\omega_i$), respectively. Next, we substitute the ansatz into equation 1.4, leading to the classical Orr-Sommerfeld and Squire equations [Orr, 1907, Sommerfeld, 1909, Squire, 1933, Schmid and

[Henningson, 2001](#)],

$$\left[-i\omega \begin{pmatrix} k^2 - \mathcal{D}^2 & 0 \\ 0 & 1 \end{pmatrix} + \begin{pmatrix} \mathcal{L}_{OS} & 0 \\ i\beta U' & \mathcal{L}_{SQ} \end{pmatrix} \right] \begin{pmatrix} \tilde{v} \\ \tilde{\eta} \end{pmatrix} = 0, \quad (1.6)$$

where \mathcal{L}_{OS} and \mathcal{L}_{SQ} refers to the Orr-Sommerfeld and Squire operators given as,

$$\mathcal{L}_{OS} = i\alpha U(k^2 - \mathcal{D}^2) + i\alpha U'' + \frac{1}{Re}(k^2 - \mathcal{D}^2)^2, \quad (1.7a)$$

$$\mathcal{L}_{SQ} = i\alpha U + \frac{1}{Re}(k^2 - \mathcal{D}^2). \quad (1.7b)$$

$k^2, \mathcal{D}, U', U''$ denotes the sum of squared wavenumbers, $k^2 = \alpha^2 + \beta^2$, differential operator in y , first- and second- derivative of the laminar velocity, respectively. Equation (1.6) is simply an eigenvalue problem which could be represented as,

$$\mathbf{L}\tilde{\mathbf{q}} = i\omega \mathbf{M}\tilde{\mathbf{q}} \quad (1.8)$$

where,

$$\mathbf{L} = \begin{pmatrix} \mathbf{L}_{OS} & 0 \\ i\beta U' & \mathcal{L}_{SQ} \end{pmatrix}, \quad \mathbf{M} \begin{pmatrix} k^2 - \mathcal{D}^2 & 0 \\ 0 & 1 \end{pmatrix}, \quad \tilde{\mathbf{q}} = \begin{pmatrix} \tilde{v} \\ \tilde{\eta} \end{pmatrix}. \quad (1.9)$$

and $i\omega$ refers to the eigenvalue. The aim of linear stability analysis is to determine the critical Reynolds number, Re_c , which is defined as the lowest value of Re over α and β , such that $Im[\omega] = 0$. For $Re > Re_c$, perturbations could grow exponentially, departing from the laminar state. In other words, we consider the behaviour of each $\alpha - \beta$ mode independently, herein referred to as *modal* analysis. Squire's theorem implies that for any unstable three-dimensional perturbations, $\beta \neq 0$, there exist an unstable two-dimensional perturbation, $\beta = 0$ with a lower Re_c [[Squire, 1933](#)]. Therefore, the unstable perturbations of wall-bounded shear flows at Re_c must be two-dimensional. The theoretical calculations was first perform by [Tollmien \[1928\]](#) and [Schlichting \[1933\]](#) for a flat-plate boundary layer flow, yielding a critical Reynolds number based on streamwise distance x of $Re_{x,c} = Ux_c/\nu = 520$ [[Schlichting and Gersten, 2017](#)]. In their honour, the unstable two-dimensional perturbations of the Orr-Sommerfeld operator is referred to as Tollmien-Schlichting (T.S) waves. For plane Poiseuille flow [[Orszag, 1971](#)] with a critical wavenumber of $\alpha_c = 1.02$. However, turbulence in plane Poiseuille flows have been observed at much lower Reynolds number, $Re \sim 1000 - 2000$, contradicting the results from linear stability analysis. Likewise, the onset of turbulence appear near $Re_{x,c} \approx 5 \times 10^5$ for flat plat boundary layer. A similar result holds for the plane Couette flow [[Meseguer and Trefethen, 2003](#)]. Despite its limitation, linear analysis analysis succeeds in predicting the critical Rayleigh number in Rayleigh-Bénard convection.

Non-modal stability

One of a major limitation of linear stability analysis considered above is that it treats each eigenmode independently, referred to as *modal* analysis. However, the interaction between decaying eigenmodes

may lead to a short-term amplification of perturbations, before eventually decaying. This phenomenon is referred to as *transient growth*, and the method of analysis is referred to as *non-modal* analysis, related to the normality of the linear Orr-Sommerfeld operator [Schmid, 2007]. To demonstrate an

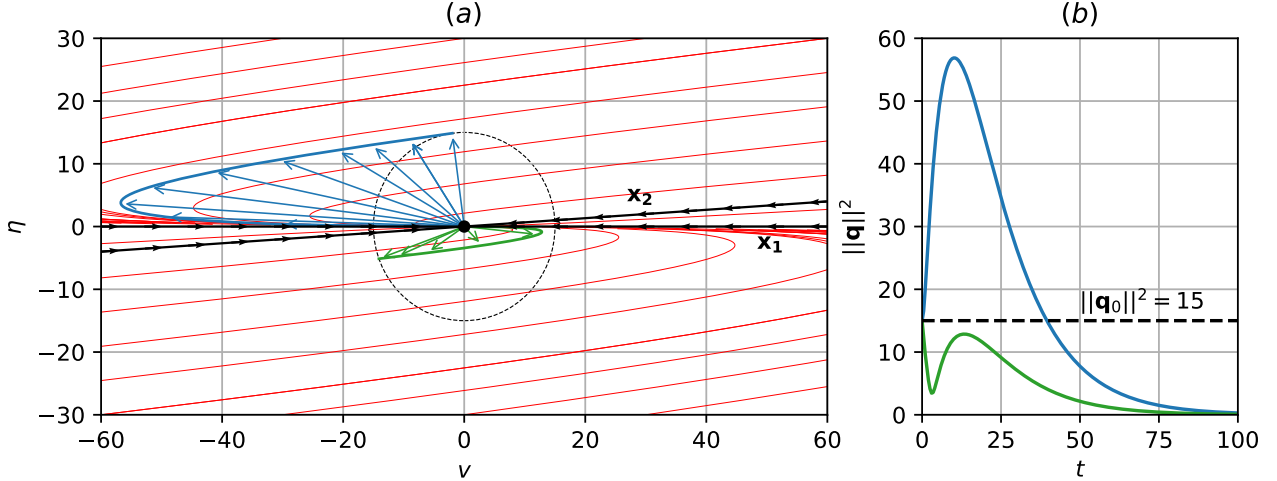


Figure 1.4: (a) The phase portrait of the toy model with $Re = 15$, (b) Transient growth.

example of transient growth, we consider a two-dimensional toy model governing the time-evolution of \mathbf{q} ,

$$\frac{d}{dt} \begin{pmatrix} v \\ \eta \end{pmatrix} = \begin{pmatrix} -\frac{1}{Re} & -1 \\ 0 & -\frac{2}{Re} \end{pmatrix} \begin{pmatrix} v \\ \eta \end{pmatrix}, \quad (1.10)$$

where Re refers to the Reynolds number. The toy model has negative eigenvalues, $(\lambda_1, \lambda_2) = (-1/Re, -2/Re)$, and unit eigenvectors $\mathbf{x}_1 = (1, 0)$, $\mathbf{x}_2 = \frac{1}{\sqrt{Re^2+1}}(Re, 1)$. Judging from the negative eigenvalues, we conclude that $\mathbf{q}(t)$ will decay exponentially. However, as $Re \rightarrow \infty$, they become increasingly non-orthogonal approaching each other such that the angle between \mathbf{x}_1 and \mathbf{x}_2 tends towards 0. At $Re = 15$, the eigenvector pairs, \mathbf{x}_1 and \mathbf{x}_2 , are highly non-orthogonal, becoming almost linearly dependent shown in figure 1.4(a). For a randomly selected initial condition with an energy-norm of $\|\mathbf{q}_0\|_2 = 15$, where $\|\cdot\|_2$ refers to the L2-norm, the trajectory in green decays exponentially for $t \in [0, 100]$ in figure 1.4(b). In contrast, for a specifically chosen initial condition shown as the blue trajectory, $\|\mathbf{q}\|_2$ is amplified nearly four times before decaying exponentially. The toy model demonstrates the significance of transient growth for a specifically chosen initial condition.

The goal of non-modal stability analysis is to search over all initial conditions, $\tilde{\mathbf{q}}_0$, leading to the maximum amplification factor at time t , resulting in an optimisation problem,

$$G(t) = \max_{\tilde{\mathbf{q}}_0 \neq 0} \frac{\langle \tilde{\mathbf{q}}(t), \tilde{\mathbf{q}}(t) \rangle}{\langle \tilde{\mathbf{q}}_0, \tilde{\mathbf{q}}_0 \rangle}, \quad \text{s.t. } \langle \tilde{\mathbf{q}}_0, \tilde{\mathbf{q}}_0 \rangle = 1, \quad (1.11)$$

where, $\langle \cdot, \cdot \rangle$ refers to the inner-product defined as,

$$\langle \mathbf{x}, \mathbf{y} \rangle = \int_{\Omega} \mathbf{x}^H \mathbf{y} \, d\Omega, \quad (1.12)$$

and \mathbf{x}^H refers to the complex conjugate transpose of \mathbf{x} . By considering the linearised operator of

(1.6), we can define a linear time invariant operator given as,

$$\tilde{\mathbf{q}}(t) = \mathcal{A}(t)\tilde{\mathbf{q}}_0, \quad (1.13)$$

which takes the solution from initial conditions, $\tilde{\mathbf{q}}_0$, to $\tilde{\mathbf{q}}(t)$ at time t . Substituting the expression above into equation (1.11),

$$G(t) = \max_{\tilde{\mathbf{q}}_0 \neq 0} \frac{\langle \mathcal{A}(t)\tilde{\mathbf{q}}_0, \mathcal{A}(t)\tilde{\mathbf{q}}_0 \rangle}{\langle \tilde{\mathbf{q}}_0, \tilde{\mathbf{q}}_0 \rangle} = \langle \tilde{\mathbf{q}}_0, \mathcal{A}^\dagger(t)\mathcal{A}(t)\tilde{\mathbf{q}}_0 \rangle = \lambda_{max}(\mathcal{A}^\dagger\mathcal{A}) \quad (1.14)$$

where $\mathcal{A}^\dagger(t)$ refers to the adjoint of $\mathcal{A}(t)$. The maximum amplification factor $\max G(t)$ is the largest eigenvalue, λ_{max} , of $\mathcal{A}^\dagger\mathcal{A}$, and the eigenvalue problem is given as,

$$\mathcal{A}^\dagger(t)\mathcal{A}(t)\tilde{\mathbf{q}}_0 = \lambda\tilde{\mathbf{q}}_0, \quad (1.15)$$

where $\tilde{\mathbf{q}}_0$ refers to the eigenvector denoting the optimal initial condition. For a detailed derivation of the optimal initial conditions or forcing, the reader is referred to [Butler and Farrell, 1992, Schmid, 2007]. An alternative method of computing transient growth is computing the pseudospectral of linear operators discussed in [Trefethen, 1997], outside the scope of this thesis.

Both two-dimensional, $\beta = 0$, and three-dimensional, $\beta \neq 0$, non-modal stability analysis have been studied.

In the two-dimensional form, the optimal initial conditions are in the form of near wall vortices tilted upstream, transiently energised referred to as the Orr-mechanism [Orr, 1907, Farrell, 1988, Reddy et al., 1993]. In the three-dimension form, streamwise vortices, acting as optimal initial conditions lead to the optimal response in the form of streamwise streaks [Reddy and Henningson, 1993]. Contrary to linear stability analysis which confers two-dimensional perturbations as linearly unstable, the key result in this analysis is that three-dimensional initial conditions, $\alpha = 0$, confer the optimal initial conditions leading to large transient growth at subcritical Reynolds numbers. Figure.. shows this.

The width of the streaks happen to be robustly occur around 100 wall units, the characteristics spacing identified in many experiments [Kline, Panton, Bandybopobi]

The optimal initial conditions involve streamwise vortices which amplify streaks, related to the lift-up effect [Ellingsen and Palm, 1975, Brandt, 2014]. These modal and nonmodal mechanisms above highlight developments based on linear methods.

1.2.2 Nonlinear dynamical systems

It is well established that coherent motions defined by flow patterns that persist in space and time play an important role in the transport of momentum and heat. In parallel shear flows, these coherent structures typically appear as near-walls streaks and quasi-streamwise rollers. A persistent, quasi-periodic cycle between the regeneration of streaks and rolls, referred to as the *self-sustaining process*, appears to be a fundamental mechanism in sustaining wall-bounded turbulence *self-sustaining process* [Hamilton et al., 1995]. This mechanism is described by the generation of streaks due to quasi-streamwise rollers

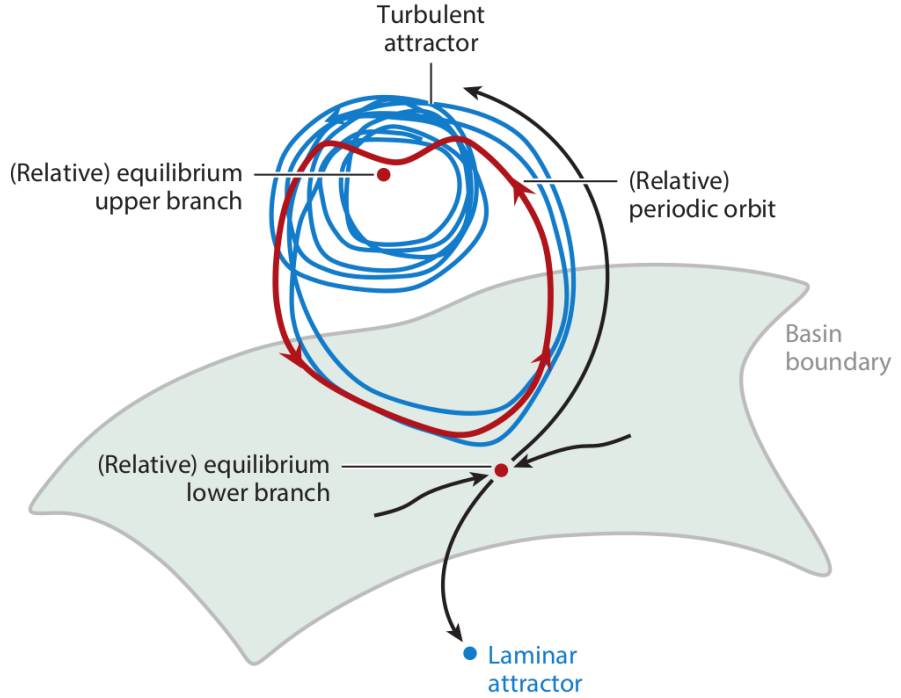


Figure 1.5: The state space organising of the upper and lower branch. Turbulence is interpreted as solution trajectories wander around the upper branch, orbiting around a network unstable invariant states. The lower branch acts as a boundary between the turbulent attractor and laminar attractor, an attracttor on the edge referred to as the edge state. Taken from [Graham and Floryan, 2021].

by redistributing the mean. These streaks become linearly unstable and breakdown, and through a nonlinear process regenerates the quasi-streamwise rollers, closing the cycle.

In the previous section, we have examined the transition process based linear mechanisms. While such mechanisms are important, the transition to turbulence is ultimately governed fully nonlinear nature of the Navier-Stokes equations. As a result, an increasing attention has been directed towards the description of turbulence as a nonlinear dynamical systems. In this view, turbulence is interpreted as a solution trajectory evolving through a phase space composed of a network such non-trivial nonlinear solutions, commonly referred to as exact coherent states (ECS) or invariant solutions [Graham and Floryan, 2021]. These invariant solutions commonly take the form of as equilibria, travelling waves, periodic and relative periodic orbits.

In the context of parallel shear flows, Nagata was the first to discover a pair of unstable equilibrium solutions in plane Couette flow by smoothly following (homotopy) from a Taylor-Couette configuration [Nagata, 1990]. This pair consist of an unstable upper branch and lower branch emerging as a saddle-node bifurcation near $Re \approx 500$, and is disconnected from the stable laminar solution. The lower branch refers to its proximity towards the stable laminar state in phase space. A travelling-wave solution in plane Couette flow also later found by the same author [Nagata, 1997]. A family of equilibrium and travelling waves solutions was found for plane Couette and plane Poiseuille flows under various boundary conditions (i.e. stress-free, slip and no-slip) where identified by [Waleffe, 2001, 2003].

While these unstable solutions demonstrate good agreements with results from DNS such as the spanwise length scales, and mean and fluctuations, they do not capture the dynamical processes. Periodic orbits defined by time-dependent solutions that have been identified in plane Couette flow [Kawahara and Kida, 2001], describing a single regeneration cycle similar to the self-sustaining process. The chaotic trajectories of turbulence have been found to be embedded within invariant solutions and their connections between them known as heteroclinic orbits, offering a robust view of the building-blocks of turbulence [Gibson et al., 2008, 2009, Viswanath, 2007, Halcrow et al., 2009, Graham and Floryan, 2021]

In the context of this transitional flows, the lower branch solution can be thought of separating the turbulent attractor from the laminar state. It's an attractor that resides on the edge of turbulence, defined as an edge state. The graphical representation of this edge is shown in figure 1.5.

1.2.3 Spatiotemporal transitional flows

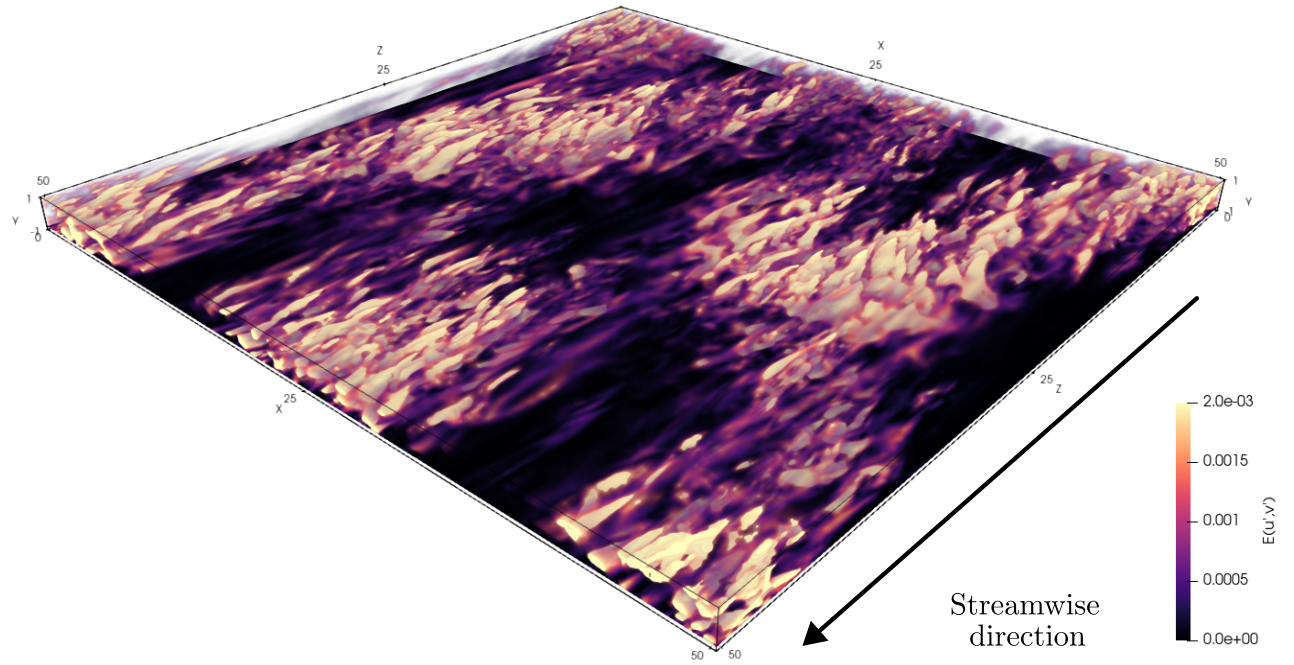


Figure 1.6: A snapshot of turbulent-laminar bands at $Re = 1400$ in a large domain $L/d = 8\pi$, depicting its spatiotemporal intermittent nature. Isovolumetric renderings are based on the spanwise, u' , and wall-normal, v' , perturbation kinetic energy, $E(u', v') = 1/2(u'^2 + v'^2)$, where the perturbation velocities are defined about the laminar state $\mathbf{u}'(\mathbf{x}, t) = \mathbf{u}(\mathbf{x}, t) - U_{lam}(y)$.

This section describes the inherent spatiotemporal intermittent description of turbulence in transitional wall-bounded shear flows commonly reported in large extended domains where the span is about fifty times the half-height of a plane Poiseuille channel, $L/h \gtrsim 50$. In this regime, turbulence

is characterised by the coexistence of turbulent and laminar structures. Examples of such are found in canonical shear flow systems such as plane Couette flows [Prigent et al., 2003, Barkley and Tuckerman, 2005, 2007, Tuckerman and Barkley, 2011, Duguet et al., 2010, Reetz et al., 2019], Taylor-Couette flows [Prigent and Dauchot, 2002, Prigent et al., 2003], pipe flows [Avila et al., 2010, 2011, Song et al., 2017, Avila et al., 2023] and plane Poiseuille flows [Tsukahara et al., 2014a,c, Tuckerman et al., 2014, Tsukahara et al., 2014b, Gomé et al., 2020, Paranjape, 2019, Paranjape et al., 2020, 2023].

We will focus on the plane Poiseuille flow configuration, where the spatiotemporal intermittent patterns are referred to as oblique turbulent-laminar bands illustrated in figure 1.6 at $Re = 1400$ for $L/h = 16\pi$. The bright and dark regions highlights coexisting spatially localised turbulent and laminar regions. These turbulent-laminar bands occur over a range of Reynolds numbers, and its precise range is likely dependent on the domain's aspect ratio [Tsukahara et al., 2014b, Tuckerman et al., 2014, Paranjape et al., 2023]. Near the upper Re threshold of this regime, the domain is fully engulfed by developed turbulent regions, referred to uniform, featureless turbulence appearing at $Re = 1800$ in figure 1.6(a). As Re decreases towards $Re = 1050$, turbulent-laminar bands persist in figures 1.7(b-f). In this region, turbulent-laminar bands angles have been observed to be inclined between $20^\circ \sim 30^\circ$, with streamwise wavelengths of $\sim 60h$, and spanwise wavelengths of $\sim 20h - 30h$ [Tsukahara et al., 2014b]. To study the preference of angles, zzz performed linear stability analysis of bands and showed that preferred angle at .. degrees. Below certain Re threshold, the spatially turbulent regions spontaneously decay where the flow relaminarises asymptotically [Tuckerman et al., 2014]. This decay is shown in $Re = 1000$ near $t = 1600$ in figure 1.7(g).

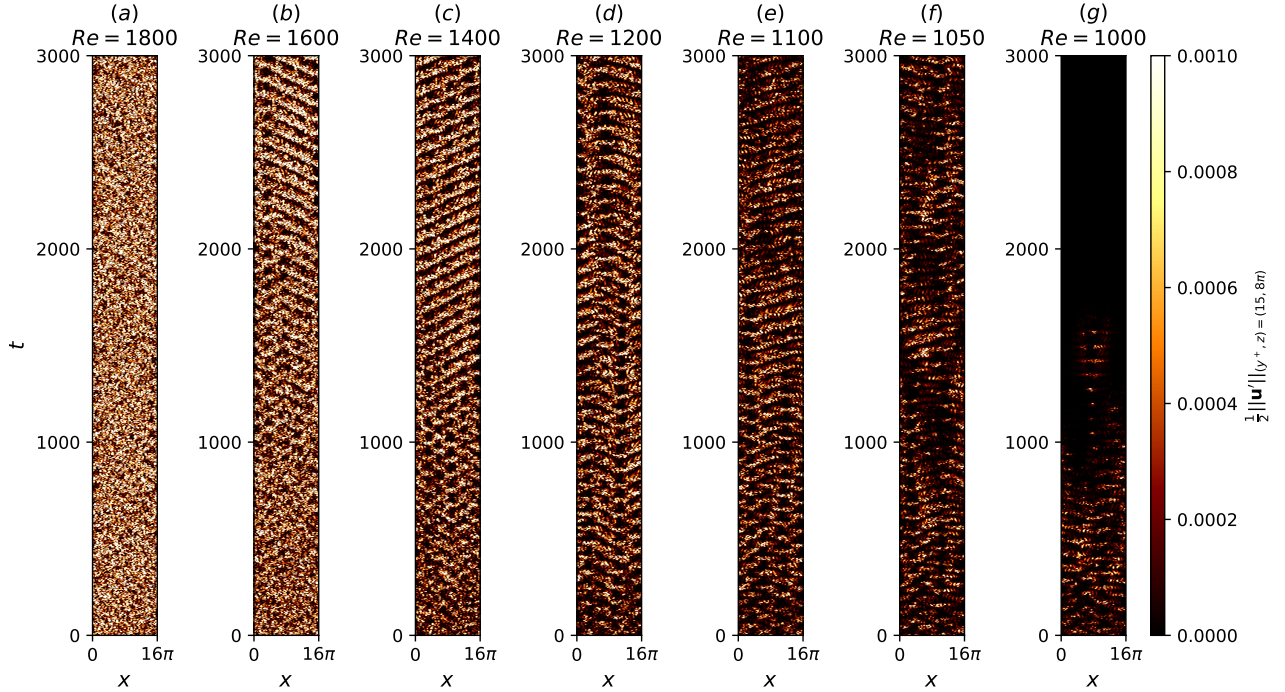


Figure 1.7: Turbulent-laminar bands for $t \in [0, 3000]$ in large domains $(L_x, L_z) = (16\pi, 16\pi)$ at (a) $Re = 1800$, (b) $Re = 1600$, (c) $Re = 1400$, (d) $Re = 1200$, (e) $Re = 1100$, (f) $Re = 1050$, (g) $Re = 1000$.

Inspired from previous studies of turbulent-laminar bands in plane Couette flows [Barkley and

Tuckerman, 2005, Reetz et al., 2019], narrow domains, titled orthogonally to the band angles where considered to investigate their dynamics [Tuckerman et al., 2014, Paranjape et al., 2020, 2023]. In narrow-tilted domains inclined at 24° , the turbulent-bands convect at about $\sim 1\%$ of the bulk velocity, propagating either upstream or downstream, above or below an critical $Re \sim 1000$, independent of domain sizes for $L_z \geq 100h$ [Tuckerman et al., 2014, Gomé et al., 2020]. The characteristic spanwise

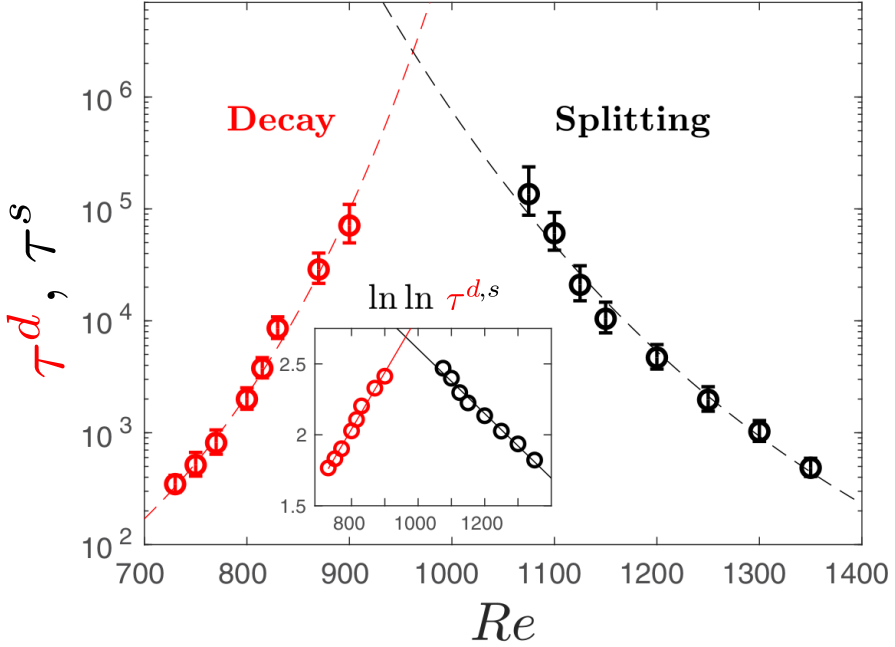


Figure 1.8: The mean decay times (red), τ^d , and mean splitting times (black), τ^s , as a function of Reynolds number, leading to a crossover point at $Re \approx 965$, adapted from [Gomé et al., 2020].

wavelengths of turbulent-laminar bands are dependent on Re , appearing at $\lambda_z \sim 20h$ for $Re \geq 1400$ and $\lambda_z \sim 40h$ for $Re \leq 1100$. Indeed, between $1300 < Re < 1400$ the bands appear to alternative between two different band-widths [Tuckerman et al., 2014], merging and splitting continuously. This points towards a band splitting event in between $Re = 1100$ and $Re = 1400$, reminiscent of a puff splitting in pipe flows [Avila et al., 2011].

On the other hand, turbulent bands appear to decay at $Re = 830$ [Gomé et al., 2020], and at $re = 1100$ but surviving for $re = 1000$ [Tuckerman et al., 2014], suggesting that turbulent bands decay spontaneously. [Gomé et al., 2020] computed the probabilities distributions of turbulent band decay, $P(\Delta t^d)$, where Δt^d refers to the time it takes for decay. One of the key insight is that the probability distributions of turbulent band decay mimicks a memoryless Poisson distribution,

$$P(\Delta t^d) = \exp(-\Delta t^d/\tau^d(Re)), \quad (1.16)$$

where $\tau^d(Re)$ refers to the mean lifetime for decay as a function of Re . Similarly, the probability distribution for band splitting also follows a Poisson distribution, $P(\Delta t^s) = \exp(-\Delta t^s/\tau^s(Re))$, where $\tau^s(Re)$ refers to the mean lifetime of a splitting event dependent on Re . The mean survival lifetime of a band decaying, τ^d , and splitting, τ^s , depends superexponentially on Re , i.e. $\tau^{d,s} = \exp(\exp(Re))$. This superexponential dependence is presented in figure 1.8, with a crossover point

at $Re_{cross} \approx 965$. This crossover point refers to equal mean survival lifetime of a band de suggesting a critical Re for the onset of turbulent bands. While there has substantial progress made towards understanding the behaviour of periodic turbulent-laminar bands in narrow-tilted domains, recently studies of isolated turbulent bands (ITBs) indicate differed behaviour. Notably, ITBs persist at $Re \approx 700$ for $t = 10000$ (far beyond figure 1.8, characterised by streak generating head, and a diffusive upstream tail. [Xiong et al., 2015, Tao et al., 2018, Shimizu and Manneville, 2019, Xiao and Song, 2020].

1.3 Rayleigh-Bénard convection

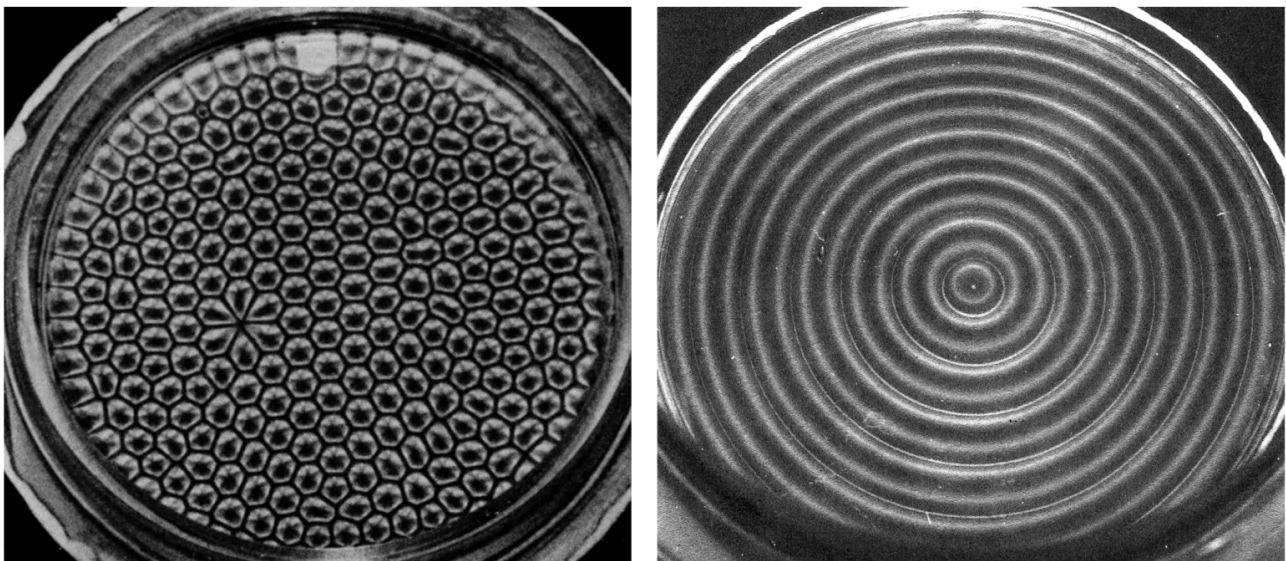


Figure 1.9: (a) Surface tension driven convection leading to the onset of hexagonal Bénard cells in a thin layer of silicone oil, heated from below and cooled by ambient air. A diamond defect appears, likely caused by plate imperfections. (b) Buoyancy driven convection in rigid plates, resulting to concentric convection rolls at 2.9 times the critical Rayleigh number. Both experiments were performed by Koschmieder and Pallas [1974], and the convection patterns were illuminated by aluminum powder, where the dark and bright regions refer to vertical and horizontal motions resepctively. These higher resolution images were taken from [Van Dyke and Van Dyke, 1982].

Rayleigh-Bénard convection (RBC) is a paradigmatic fluid configuration describing the motion of the fluid confined between two infinite-parallel plates heated from below and cooled from the top. As the bottom plate is heated, the bottom layer fluid becomes more buoyant and tends to rise, while the colder top fluid layer is becomes relatively less buoyant and tends to sink, leading to an overturning of layers. Viscous forces between neighbouring fluid parcels act to resist the motion. As buoyancy overcomes these viscous forces, the fluid layers overturn, resulting in the initiation of buoyancy-driven convection, the physical mechanism underpinning RBC.

One of the earliest experimental studies dedicated to buoyancy-driven convection was conducted by Henri Bénard [Bénard, 1901], who observed the formation of hexagonal convection cells above a certain temperature threshold ΔT . These hexagonal patterns are referred to as Bénard cells are illustrated in figure 1.9(a) (adapted from [Koschmieder and Pallas, 1974]). Subsequently, Rayleigh

[1916] carried out one of first linear stability analyses of buoyancy-driven convection, predicting the onset of convection at a critical Rayleigh number of $Ra_c = 657.5$. However, Rayleigh's analysis assumed an idealised free-free boundary conditions, which differed from the rigid-free setup of Bénard's experiment. The linear stability analysis for rigid-free configuration was later performed by Jeffreys [1928] yielding a higher critical Rayleigh number of $Ra_c = 1058$. In the rigid-rigid configuration, the critical Rayleigh number increases further to $Ra_c = 1708$ [Pellew and Southwell, 1940]. The Rayleigh number in Bénard's original experiment was found to be 300 to 1500 smaller than Ra_c for the free-free and rigid-free cases [Wesfreid, 2017]. This contradiction, not recognised by Bénard at the time, lies in the significant role of surface tension in thin fluid layers exposed to air, now known as Bénard-Maragoni (BM) convection [Block, 1956, Cloot and Lebon, 1984, Manneville, 2006, Wesfreid, 2017]. In BM convection, fluid motion is primarily driven by surface tension gradients due to variations of temperature, forming hexagonal cells, as in figure 1.9(a). The preference for hexagonal cells in BM convection was later confirmed based on weakly nonlinear stability analysis [Cloot and Lebon, 1984]. As the fluid layer becomes thicker, surface-tension effects diminish and buoyancy-driven convection becomes dominant. Similarly, placing a rigid lid on top of a thin fluid layer suppresses surface-tension effects, also resulting in buoyancy-driven convection. The preferred convection patterns based on weakly nonlinear stability analysis are the two-dimensional parallel rolls, now referred to as ideal straight rolls (ISRs) [Schlüter et al., 1965, Bodenschatz et al., 2000]. In circular containers, the ISRs conform to the geometry of the boundaries, forming concentric convection rolls illustrated in figure 1.9(b). Interestingly, hexagonal cells have been observed in buoyancy-driven flows of non-Boussinesq fluids [Hoard et al., 1970, Bodenschatz et al., 2000]. In this thesis, I will consider RBC with rigid-rigid boundary conditions with for which the critical Rayleigh number is $Ra_c = 1708$. Notably, the corresponding critical wavelength is $q_c = 3.12/d$ (or $\lambda_c \approx 2d$), suggesting that distance separating the plates, d , dictates the length of a single roll, $l_{roll} = \lambda_c/2 \approx d$.

As mentioned earlier, stationary ISRs near q_c emerge just above Ra_c , based on weakly nonlinear stability analysis. [Eckhaus, 1965, Schlüter et al., 1965]. However, this prediction contradicted by the emergence of time-dependent oscillatory ISRs in experiments [Rossby, 1969, Willis and Deardorff, 1970] at $Ra = 9200$ (or roughly five times Ra_c), where weakly nonlinear stability becomes inapplicable far from threshold. To address this, a direct secondary stability analysis was employed to study the stability of ISRs further from Ra_c , based on Galerkin analysis [Busse, 1972]. The results from the analysis is described by the Busse balloon, which illustrates the stability boundaries of ISRs as a function of Ra and Pr and roll wavenumber, α , shown figure 1.10 [Busse, 1978]. The boundaries of the Busse balloon are described by a range of secondary instabilities, each arising from different physical mechanisms [Busse, 1978]. At large Prandtl numbers, $Pr = O(10^2)$, the zig-zag (ZZ) and cross-roll (CR) instabilities delimits the balloon for small and large roll wavenumbers. The zig-zag instabilities cause zig-zag undulations while the CR instabilities generates rolls orthogonal to the underlying ISR structure, effectively increasing or decreasing the roll wavenumber respectively [Busse and Whitehead, 1971]. Examples of these instabilities at $Pr = 100$ are illustrated in figure 1.11(a,b).

At moderate Prandtl numbers, $Pr = O(1)$, the Busse balloon is bounded by the skewed varicosed (SV) for high roll wavenumbers and the oscillatory (OS) instability at large Ra . The skewed-varicosed

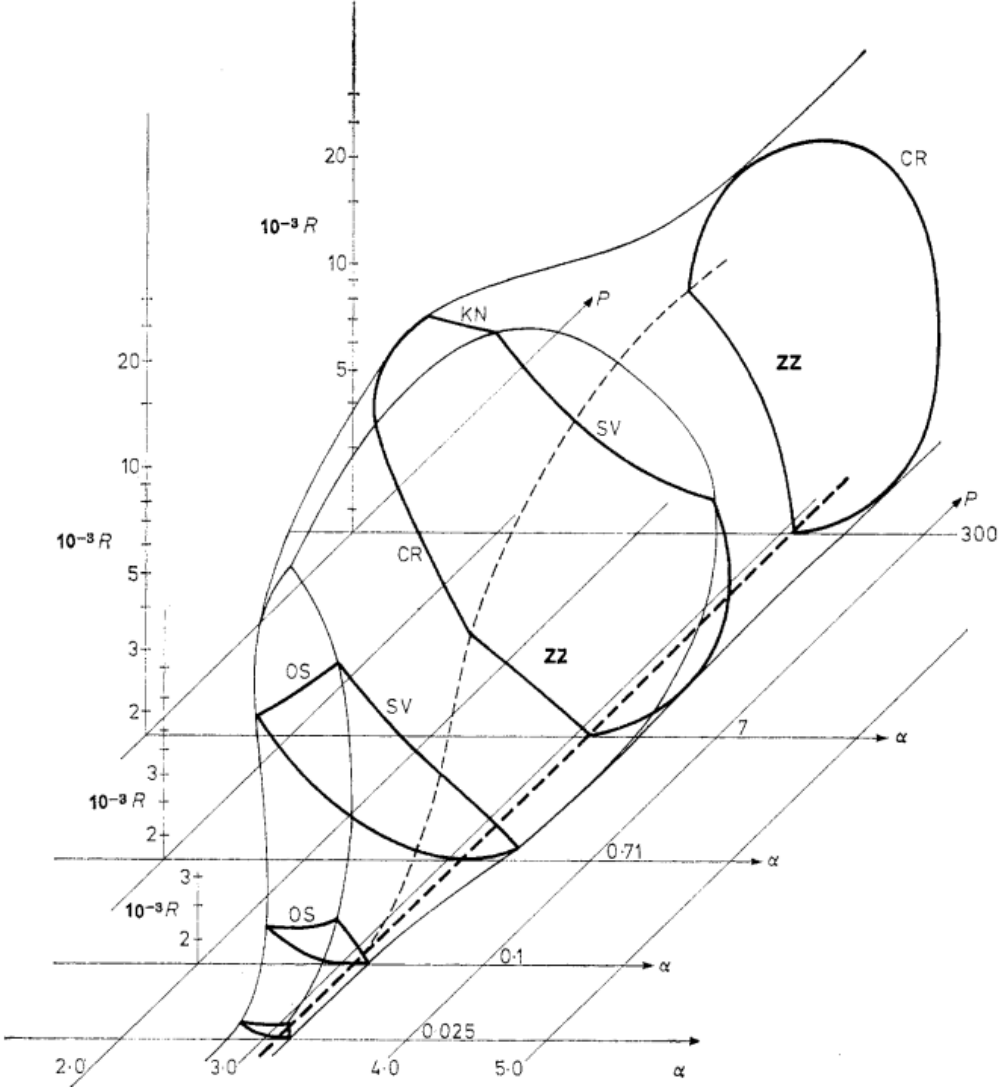


Figure 1.10: The Busse balloon describes the stability boundaries of ISRs in a $\varepsilon - q$ space. For larger wavenumbers, the instability mechanism is described by the skewed-varicose (SV) instability. For smaller wavenumbers, the instability mechanism is described by the Eckhaus instability. For large ε , the instability is described by the onset of oscillatory instability. Busse balloon digitised from [Plapp, 1997] for $Pr \approx 1$.

(SV) instability leads to roll-pinchig where pinched rolls merged into a single roll, reducing roll wavenumber while the oscillatory instability leads to the onset of an oscillatory ISRs. Examples of the respective instabilities at $Pr = 1$ are shown in figure 1.11(c,d). At higher wavenumbers, the skewed varicose (SV) instability becomes relevant at intermediate Prandlt numbers, characterised by roll pinching and merging that effectively reduces the roll wavenumber. Finally, the Eckhaus instability (not shown), related to the symmetry of the system, appears close to the Ra_c , leading a disturbance parallel to the underlying rolls which either creates or destroy rolls such that the resultant roll wavenumber adheres to the stability boundaries [Lowe and Gollub, 1985]. Near $Pr = 1$, the Eckhaus instability coincides with the crossroll instability (figure 6 from Bodenschatz et al. [2000], adapted from Plapp [1997].) In this thesis, we focus on fluids with $Pr = 1$, where the skewed-varicose, Eckhaus and cross-roll instabilities typically arises. The stability boundaries of the Busse

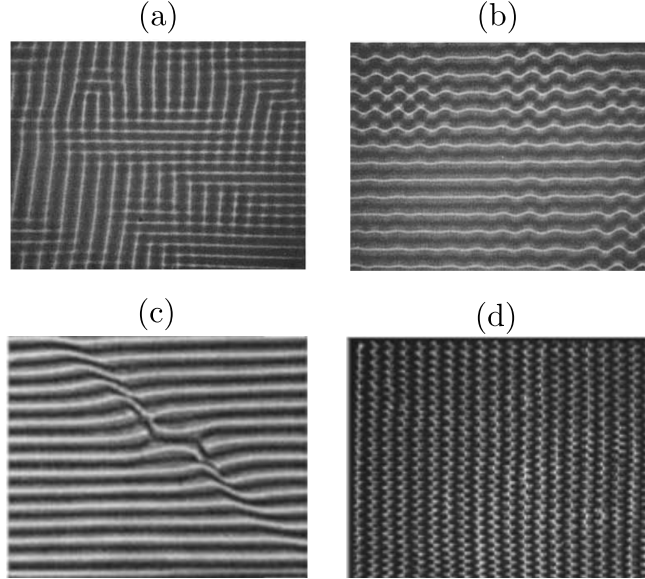


Figure 1.11: ISRs experiencing (a) cross-roll instability at $Ra = 3000, Pr = 100$ and (b) zig-zag instability at $Ra = 3600, Pr = 100$ [Busse and Whitehead, 1971]. (c) Skew-varicosed instability at $Ra = 5568, Pr = 1$ [Plapp, 1997], and (d) oscillatory instability at $Ra = 10384, Pr = 1$ [Cakmur et al., 1997a].

balloon have been experimentally verified [Busse and Whitehead, 1971, Croquette, 1989a, Plapp, 1997]. However, the exact roll wavenumbers of ISRs exhibits hysteresis. As Ra is continuously modified, the ISRs with wavenumbers that are outside of the stability boundaries of the Busse balloon, undergo spontaneous rolls dislocations from various secondary instabilities described above. These instabilities either increase or decrease the roll wavenumber, adhering to the the stability boundaries of the Busse balloon. The hysteretic behaviour indicates that the roll wavenumber of the ISRs is strongly dependent on the system's history [Bodenschatz et al., 2000].

It is worth noting that the solutions in the form of ISRs appear to be an exception rather than the rule [Croquette, 1989b]. The coexistence of multiple ‘non-ISR’ states, in the form of squares, travelling/stationary targets, giant rotating spirals, and oscillatory convection patterns have been found over several years [Le Gal et al., 1985, Croquette, 1989a, Plapp, 1997, Hof et al., 1999, Rüdiger and Feudel, 2000, Borońska and Tuckerman, 2010a,b]. Investigation of cylindrical RBC with small aspect-ratio ($\Gamma = 2$) found eight stationary states (at the same $Ra = 142000$), and two oscillatory states ($Ra > 14200$) [Hof et al., 1999]. These findings were later supported by numerical experiments and bifurcation analyses [Ma et al., 2006, Borońska and Tuckerman, 2010a,b]. In particular, bifurcation analyses performed by Ma et al. [2006], revealed twelve stable branches in the form of symmetric and asymmetric convection rolls near onset ($Ra \leq 2500$), with the potential emergence of hundreds of branches at higher Rayleigh numbers, $Ra \leq 30000$ [Borońska and Tuckerman, 2010b].

In larger domains ($\Gamma \geq 28$), giant rotating spirals were identified and thoroughly investigated [Plapp and Bodenschatz, 1996, Plapp et al., 1998]. Experimental and numerical studies of RBC with varying sidewall boundary conditions (i.e. thermally insulating, conducting an no-slip) [Tuckerman and Barkley, 1988, Siggers, 2003, Paul et al., 2003, Bouillé et al., 2022], non-Boussinesq convection [Bodenschatz et al., 1992], and rotational effects [Hu et al., 1997] were investigated, where multiple

states were also reported. More recently, Reetz and Schneider [2020], Reetz et al. [2020] computed up to sixteen stable and unstable invariant states and identified heteroclinic orbits between the multiple states in an inclined RBC. The existence of multiple stable states apart from ISRs suggest that RBC forms a multiple bistable systate above Ra_c . To complicate matter further, an intrinsic chaotic state of convection was discovered.

In the late 1990s, convection rolls exhibiting spatio-temporal chaotic behaviour known as spiral defect chaos (SDC) are found in the same stability boundaries where ISRs were expected [Morris et al., 1993, Hu et al., 1993, Decker et al., 1994, Hu et al., 1995, Morris et al., 1996, Cakmur et al., 1997a, Ahlers, Egolf et al., 1998, 2000, Chiam et al., 2003, Vitral et al., 2020]. Notably only carefully prepared experiment setups led to ISRs while uncontrolled initial conditions yield SDC. It is well established that SDC exists as intrinsic attractor of RBC, independent of sidewall conditions Morris et al. [1996], forming a bistable system with ISRs [Cakmur et al., 1997a] across a range of Ra at Pr illustrated in figure 1.12. However, the SDC attractor have been found to be unstable at $Pr = 4$, decaying towards

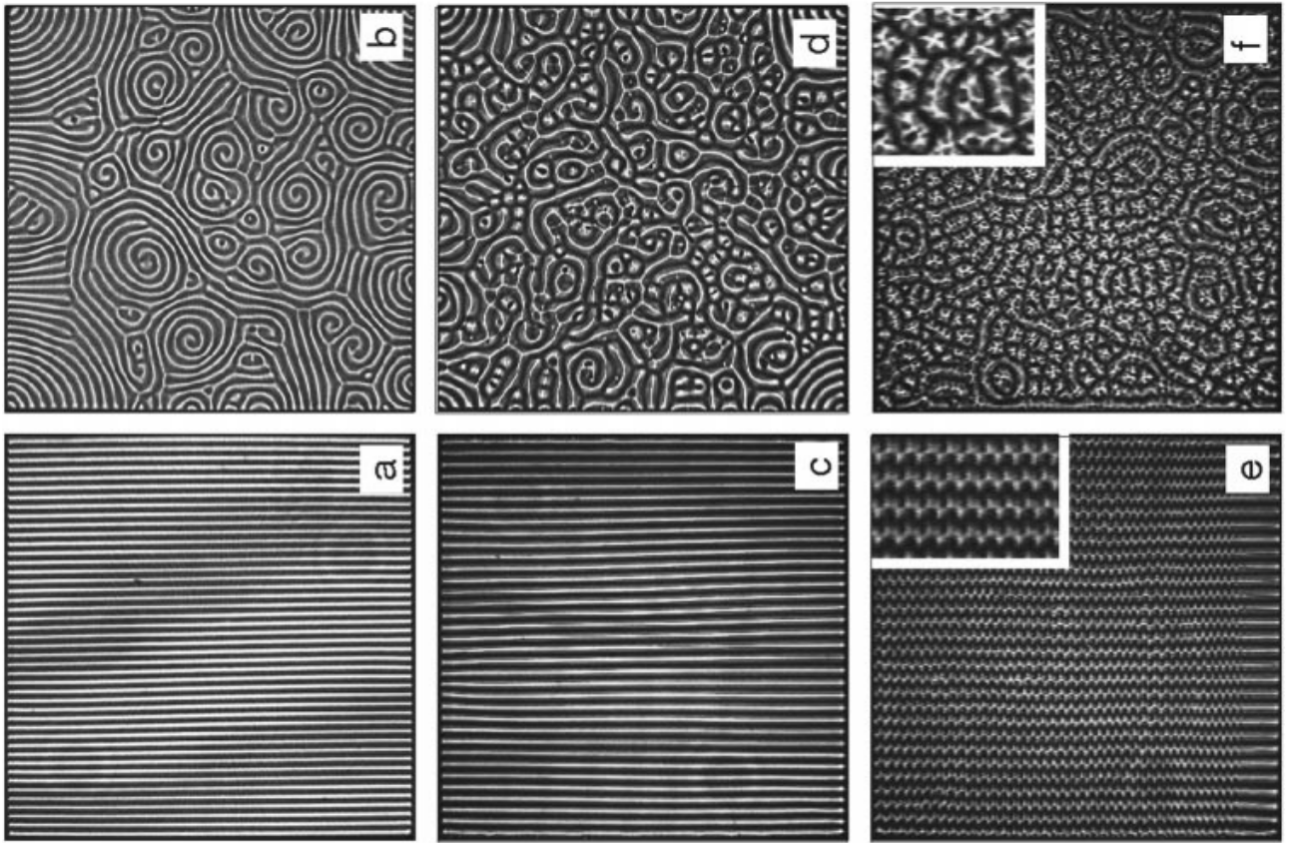


Figure 1.12: The coexistence of spiral defect chaos (SDC, top row) and ideal straight rolls (ISRs, bottom row) at (a,b) $Ra = 3279$, (c,d) $Ra = 6832$ and (e,f) $Ra = 10384$. The domain size is $\Gamma = 50$ and $Pr = 1$, adapted from Cakmur et al. [1997a].

ISRs over long periods [Bajaj et al., 1997]. SDC has also been modelled in numerical simulations of the two-dimensional Swift-Hohenberg equations [Swift and Hohenberg, 1977, Xi et al., 1993, Xi and Gunton, 1995, Schmitz et al., 2002, Karimi et al., 2011]. The critical Rayleigh number for the onset of SDC, Ra_s , depends on the domain's aspect ratio, and Prandtl number [Hu et al., 1995, Bajaj et al., 1997, Cakmur et al., 1997b, Bodenschatz et al., 2000], and remain inconclusive. Notably, SDC

has been reported in large domains ($\Gamma \gtrsim 20$), implying that there is a minimal Γ for SDC to occur [Bodenschatz et al., 2000], supporting the dependence of the Ra_s on Γ . The chaotic properties of SDC is also dependent of aspect ratio, where the leading Lyapunov exponents decreases with aspect ratio [Egolf et al., 2000, Paul et al., 2007]. Investigations into the spatial-temporal description of SDC such as the averaged roll-curvature Hu et al. [1995], probability distribution of spirals Ecke et al. [1995], Liu and Ahlers [1996] and correlation length-/time-scales [Morris et al., 1993, 1996, Cakmur et al., 1997b] have been undertaken. Specifically, the correlation length-scales [Morris et al., 1993, 1996, Cakmur et al., 1997b] scales exponentially with Ra , suggesting that onset of SDC from ISRs mimicks a phase transition. Spatiotemporal chaotic behaviour similar to SDC has been found also in other pattern-formation systems such as rotational RBC Hu et al. [1997], dielectric barrier discharge Dong et al. [2005] and advection diffusion reaction systems Affan and Friedrich [2014].

1.4 Rayleigh-Bénard Poiseuille (RBP) flows

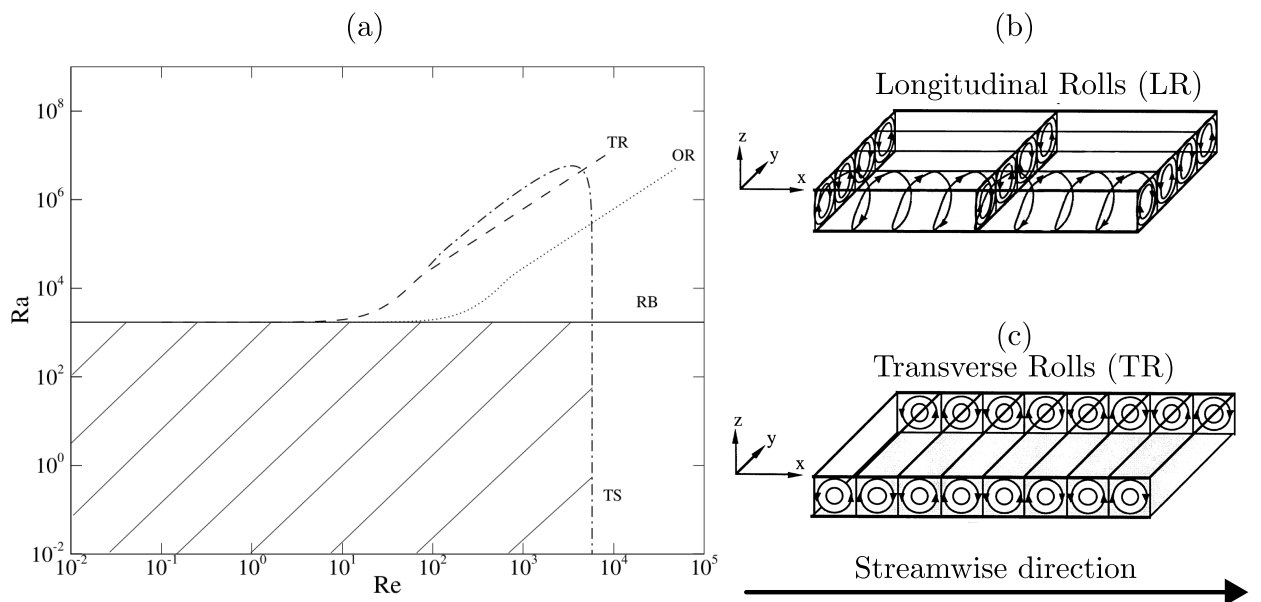


Figure 1.13: (a) Neutral stability curves of longitudinal rolls (LR), oblique rolls (OR), transverse rolls (TR) and Tollmien-Schlichting (TS) waves, adapted from John Soundar Jerome et al. [2012]. The shaded area refers to damped perturbations. Sketch of (b) longitudinal and (c) transverse rolls, adapted from Kelly [1994].

The neutral stability curves in the Rayleigh-Bénard Poiseuille (RBP) comprising of both plane Poisueuille flow (PPF) and Rayleigh-Béanrd convection (RBC) systems, are bounded by the onset of Tollmien-Schlichting waves at $Re_c = 5772.22$ [Orszag, 1971], and by the onset of convection rolls at $Ra_c = 1708$ [Pellew and Southwell, 1940], respectively. The imposed mean Poiseuille flow in the RBP system breaks the rotational invariance of the convection rolls, categorising them based on their orientation to the mean flow direction, namely: longitudinal ($\alpha = 0, \beta \neq 0$), transverse ($\alpha \neq 0, \beta = 0$) and oblique rolls ($\alpha \neq 0, \beta \neq 0$). The primary instabilities leading to these rolls were first investigated by Gage and Reid [1968] in an infinitely extended layer. For the onset of longitudinal rolls, the linearised system reduces to that of RBC. Hence, the critical Rayleigh number

for the onset of longitudinal rolls remains the same, $Ra_{\parallel} = Ra_c = 1708.8$ with a critical wavenumber, $\alpha_{\parallel} = \alpha_c = 3.13$ [Pellew and Southwell, 1940, Kelly, 1994], independent of both Reynolds number, Re , and Prandtl number Pr . In contrast, the onset of transverse rolls exhibits a critical Rayleigh number, $Ra_{\perp} = f(Re, Pr)$, that increases with Re and is dependent on Pr [Gage and Reid, 1968, Müller et al., 1992, Nicolas et al., 1997]. The critical Rayleigh number for the onset of oblique rolls can be obtained by applying a Squire transformation [Squire, 1933] to the linearised problem for transverse rolls. For a given Ra , the corresponding critical Re for the onset of oblique rolls is higher than that of transverse rolls [Gage and Reid, 1968]. The neutral stability curves associated with the transverse rolls (TR), oblique rolls (OR) and longitudinal rolls (LR) are shown in figure 1.13.

Experimental observations of the onset of longitudinal rolls have been reported in channels with large transverse aspect ratios (i.e span-to-depth) [Akiyama et al., 1971, Ostrach and Kamotani, 1975, Fukui et al., 1983], while the onset of transverse rolls are observed in narrower channels [Luijx et al., 1981, Ouazzani et al., 1989, 1990]. Indeed, linear stability analysis conducted for finite channels revealed that critical Rayleigh number Ra_{\parallel} remains independent for transverse aspect ratios greater than five, and increases quickly below that. Therefore, the critical Rayleigh number for onset of transverse rolls, Ra_{\perp} , is lower than Ra_{\parallel} in narrow channels for small Reynolds numbers [Nicolas et al., 2000], providing support for the preference of transverse rolls in narrow channels. Ouazzani et al. [1990] reported laminar Poiseuille flow in the Ra, Re parameter space where transverse rolls are expected based on temporal linear stability analysis. This contraction was addressed by Müller et al. [1992], who showed that transverse rolls can be either convectively or absolutely unstable, and the boundary between them matches with the experimental results of Ouazzani et al. [1990]. By considering the response from three-dimensional impulse, Carrière and Monkewitz [1999] further demonstrated that the longitudinal rolls, unlike the transverse rolls, are always convectively unstable. Nonmodal stability analysis of subcritical RBP, $Ra < Ra_c$, $Re < Re_c$, performed by John Soundar Jerome et al. [2012] revealed that the optimal transient growth is primarily dominated by streamwise rollers of plane Poiseuille flow [Reddy and Henningson, 1993], with a spanwise wavenumber of $\beta_{opt} \approx 2.05$. The maximum amplification factor, G_{max} increases modestly with Ra , and the critical wavenumber approaches, α_{\parallel} , indicative of longitudinal rolls. Since longitudinal rolls are the dominant primary instability for $Re > 0$ in infinite domains, their secondary stability have been analysed by Clever and Busse [1991]. Their study revealed the presence of a secondary, time-dependent wavy instability near $Re \sim 100$ [Clever and Busse, 1991], leading to the onset of tertiary solutions in the form of wavy rolls. These have been observed experimentally and was found to be convectively unstable [Pabiou et al., 2003, 2005, Nicolas et al., 2010]. Clever and Busse [1991] also speculated that the wavy rolls are less efficient at transporting heating than longitudinal rolls at the same control parameters, confirmed numerically [Nicolas et al., 2012]. The impact of finite transverse aspect ratios on the onset of wavy rolls have been also studied [Xin et al., 2006, Nicolas et al., 2010], where the critical Ra was found to be approximately 1.5 times higher than that in an infinite domain Clever and Busse [1991]. The influence of external excitations on the development length of wavy rolls have been explored. An increase in external excitation amplitude have shown to reduce the required development length of wavy rolls [Nicolas et al., 2010, 2012]. More recently, studies of turbulent RBP flows showed that

shear-driven turbulence can enhance heat fluxes [Scagliarini et al., 2014, 2015, Pirozzoli et al., 2017]. Extensions of the RBP configuration, such as flows over wavy walls or with sinusoidal thermal forcing have been investigated, potentially offering a reduction in drag and enhancing heat transport [Hossain et al., 2012, Hossain and Floryan, 2016, 2020]. For a comprehensive overview of RBP flows, the reader is referred to the reviews by Kelly [1994] and Nicolas [2002].

1.4.1 Thesis Outline

In this thesis, I am particularly focused on the transition behaviour of fluid flow driven by shear and buoyancy, addressing questions related to the onset of instabilities due to shear and buoyancy, and the (possible) competitive between shear and buoyancy driven instabilities. I would like to preface that while this thesis is dealing with onset of instabilities, it does not clearly indicate that the onset of such instabilities necessarily lead to turbulence, hence, for terminology sake, we shall be looking into transitional regimes where the fluid neither laminar nor turbulent. The main motivations are two-folds, both from an academic and applied point-of-view. Within academia, the onset and transition to turbulence in Rayleigh-Bénard Poiseuille flows remains poorly understand. Whilst there had been significant progress in our understand of transition to turbulence in independent setups, Rayleigh-Bénard convection and plane Poiseuille flows, their combined effects are not known. The thesis is structured into the follow, Chapter 1 is the introduction with literature review, chapter 2 methodology assosicated with the spectral/*hp*-element method, chapter 3 with results related to the the Rayleigh and Reynolds number sweep, chapter 4 with a specific focus on the bistability between spiral defect chaos and ideal straight rolls and finally chapter 5 with concluding remarks.

1. Academic motivation - flow structures, statistics, transition.
2. Application motivation - shear, heat transfer. Chip cooling, thin-film fabrication and atmospheric boundary layer.

We seek to investigate the influence of unstable stratification quantified by Rayleigh number Ra , on the behaviour tubulent-laminar bands. The onset of convection occurs at a critical Rayleigh number of $Ra_c > 1708$, in the form of a pair of convection rolls. When aligned in the streamwise direction, the convection rolls are seemingly analogous to a pair of counter-rotating vortices, an optimal initial condition for transient growth. Our investigation naturally answers a few questions related to turbulent-laminar bands. For example, does the onset of turbulent-laminar bands, Re_{cr} decrease with increasing Ra ? Do Ra -effects influence the structure of turbulent-laminar bands i.e band angle/width?

The answers to our research will have important implications Rayleigh-Bénard Poiseuille flows, ubiquitous in atmospheric, geophysical and engineering flows.

Bibliography

Clouds streets and comma clouds near svalbard. <https://earthobservatory.nasa.gov/images/87749/clouds-streets-and-comma-clouds-near-svalbard>.

H. Affan and R. Friedrich. Spiral defect chaos in an advection-reaction-diffusion system. *Physical Review E*, 89(6):062920, June 2014. ISSN 1539-3755, 1550-2376. doi: 10.1103/PhysRevE.89.062920. URL <https://link.aps.org/doi/10.1103/PhysRevE.89.062920>.

Guenter Ahlers. Experiments on spatio-temporal chaos.

Mitsunobu Akiyama, Guang-Jyh Hwang, and KC Cheng. Experiments on the onset of longitudinal vortices in laminar forced convection between horizontal plates. 1971. ISSN 0022-1481.

Kerstin Avila, David Moxey, Alberto De Lozar, Marc Avila, Dwight Barkley, and Björn Hof. The Onset of Turbulence in Pipe Flow. *Science*, 333(6039):192–196, July 2011. ISSN 0036-8075, 1095-9203. doi: 10.1126/science.1203223. URL <https://www.science.org/doi/10.1126/science.1203223>.

Marc Avila, Ashley P. Willis, and Björn Hof. On the transient nature of localized pipe flow turbulence. *Journal of Fluid Mechanics*, 646:127–136, March 2010. ISSN 0022-1120, 1469-7645. doi: 10.1017/S0022112009993296. URL https://www.cambridge.org/core/product/identifier/S0022112009993296/type/journal_article.

Marc Avila, Dwight Barkley, and Björn Hof. Transition to Turbulence in Pipe Flow. *Annual Review of Fluid Mechanics*, 55(1):575–602, January 2023. ISSN 0066-4189, 1545-4479. doi: 10.1146/annurev-fluid-120720-025957. URL <https://www.annualreviews.org/doi/10.1146/annurev-fluid-120720-025957>.

Kapil M. S. Bajaj, David S. Cannell, and Guenter Ahlers. Competition between spiral-defect chaos and rolls in Rayleigh-Bénard convection. *Physical Review E*, 55(5):R4869–R4872, May 1997. ISSN 1063-651X, 1095-3787. doi: 10.1103/PhysRevE.55.R4869. URL <https://link.aps.org/doi/10.1103/PhysRevE.55.R4869>.

Dwight Barkley and Laurette S. Tuckerman. Computational Study of Turbulent Laminar Patterns in Couette Flow. *Physical Review Letters*, 94(1):014502, January 2005. doi: 10.1103/PhysRevLett.94.014502. URL <https://link.aps.org/doi/10.1103/PhysRevLett.94.014502>. Publisher: American Physical Society.

Dwight Barkley and Laurette S Tuckerman. Mean flow of turbulent–laminar patterns in plane Couette flow. *Journal of Fluid Mechanics*, 576:109–137, 2007. ISSN 1469-7645. Publisher: Cambridge University Press.

Myron J. Block. Surface Tension as the Cause of Bénard Cells and Surface Deformation in a Liquid Film. *Nature*, 178(4534):650–651, September 1956. ISSN 0028-0836, 1476-4687. doi: 10.1038/178650a0. URL <https://www.nature.com/articles/178650a0>.

Eberhard Bodenschatz, David S. Cannell, John R. De Bruyn, Robert Ecke, Yu-Chou Hu, Kristina Lerman, and Guenter Ahlers. Experiments on three systems with non-variational aspects. *Physica D: Nonlinear Phenomena*, 61(1-4):77–93, December 1992. ISSN 01672789. doi: 10.1016/0167-2789(92)90150-L. URL <https://linkinghub.elsevier.com/retrieve/pii/016727899290150L>.

Eberhard Bodenschatz, Werner Pesch, and Guenter Ahlers. Recent Developments in Rayleigh-Bénard Convection. *Annual Review of Fluid Mechanics*, 32(1):709–778, January 2000. ISSN 0066-4189, 1545-4479. doi: 10.1146/annurev.fluid.32.1.709. URL <https://www.annualreviews.org/doi/10.1146/annurev.fluid.32.1.709>.

Katarzyna Borońska and Laurette S. Tuckerman. Extreme multiplicity in cylindrical Rayleigh-Bénard convection. I. Time dependence and oscillations. *Physical Review E*, 81(3):036320, March 2010a. ISSN 1539-3755, 1550-2376. doi: 10.1103/PhysRevE.81.036320. URL <https://link.aps.org/doi/10.1103/PhysRevE.81.036320>.

Katarzyna Borońska and Laurette S. Tuckerman. Extreme multiplicity in cylindrical Rayleigh-Bénard convection. II. Bifurcation diagram and symmetry classification. *Physical Review E*, 81(3):036321, March 2010b. ISSN 1539-3755, 1550-2376. doi: 10.1103/PhysRevE.81.036321. URL <https://link.aps.org/doi/10.1103/PhysRevE.81.036321>.

N. Boullié, V. Dallas, and P. E. Farrell. Bifurcation analysis of two-dimensional Rayleigh-Bénard convection using deflation. *Physical Review E*, 105(5):055106, May 2022. ISSN 2470-0045, 2470-0053. doi: 10.1103/PhysRevE.105.055106. URL <https://link.aps.org/doi/10.1103/PhysRevE.105.055106>.

Luca Brandt. The lift-up effect: The linear mechanism behind transition and turbulence in shear flows. *European Journal of Mechanics - B/Fluids*, 47:80–96, September 2014. ISSN 09977546. doi: 10.1016/j.euromechflu.2014.03.005. URL <https://linkinghub.elsevier.com/retrieve/pii/S0997754614000405>.

F. H. Busse. The oscillatory instability of convection rolls in a low Prandtl number fluid. *Journal of Fluid Mechanics*, 52(1):97–112, March 1972. ISSN 0022-1120, 1469-7645. doi: 10.1017/S0022112072002988. URL https://www.cambridge.org/core/product/identifier/S0022112072002988/type/journal_article.

F H Busse. Non-linear properties of thermal convection. *Reports on Progress in Physics*, 41(12):1929–1967, December 1978. ISSN 0034-4885, 1361-6633. doi: 10.1088/0034-4885/41/12/003. URL <https://iopscience.iop.org/article/10.1088/0034-4885/41/12/003>.

F. H. Busse and J. A. Whitehead. Instabilities of convection rolls in a high Prandtl number fluid. *Journal of Fluid Mechanics*, 47(2):305–320, May 1971. ISSN 0022-1120, 1469-7645. doi: 10.1017/S0022112071001071. URL https://www.cambridge.org/core/product/identifier/S0022112071001071/type/journal_article.

Kathryn M. Butler and Brian F. Farrell. Three-dimensional optimal perturbations in viscous shear flow. *Physics of Fluids A: Fluid Dynamics*, 4(8):1637–1650, August 1992. ISSN 0899-8213. doi: 10.1063/1.858386. URL <https://pubs.aip.org/pof/article/4/8/1637/402702/Three-dimensional-optimal-perturbations-in-viscous>.

Henri Bénard. Les tourbillons cellulaires dans une nappe liquide. - Méthodes optiques d’observation et d’enregistrement. *Journal de Physique Théorique et Appliquée*, 10(1):254–266, 1901. ISSN 0368-3893. doi: 10.1051/jphystap:0190100100025400. URL <http://www.edpsciences.org/10.1051/jphystap:0190100100025400>.

Reha V. Cakmur, David A. Egolf, Brendan B. Plapp, and Eberhard Bodenschatz. Bistability and Competition of Spatiotemporal Chaotic and Fixed Point Attractors in Rayleigh-Bénard Convection. *Physical Review Letters*, 79(10):1853–1856, September 1997a. ISSN 0031-9007, 1079-7114. doi: 10.1103/PhysRevLett.79.1853. URL <https://link.aps.org/doi/10.1103/PhysRevLett.79.1853>.

Reha V. Cakmur, David A. Egolf, Brendan B. Plapp, and Eberhard Bodenschatz. Transition from Spatiotemporal Chaos to Ideal Straight Rolls in Rayleigh-Benard Convection, February 1997b. URL <http://arxiv.org/abs/patt-sol/9702003>. arXiv:patt-sol/9702003.

Philippe Carrière and Peter A. Monkewitz. Convective versus absolute instability in mixed Rayleigh–Bénard–Poiseuille convection. *Journal of Fluid Mechanics*, 384:243–262, April 1999. ISSN 0022-1120, 1469-7645. doi: 10.1017/S0022112098004145. URL https://www.cambridge.org/core/product/identifier/S0022112098004145/type/journal_article.

K.-H. Chiam, M. R. Paul, M. C. Cross, and H. S. Greenside. Mean flow and spiral defect chaos in Rayleigh-Bénard convection. *Physical Review E*, 67(5):056206, May 2003. ISSN 1063-651X, 1095-3787. doi: 10.1103/PhysRevE.67.056206. URL <https://link.aps.org/doi/10.1103/PhysRevE.67.056206>.

R. M. Clever and F. H. Busse. Instabilities of longitudinal rolls in the presence of Poiseuille flow. *Journal of Fluid Mechanics*, 229(-1):517, August 1991. ISSN 0022-1120, 1469-7645. doi: 10.1017/S0022112091003142. URL http://www.journals.cambridge.org/abstract_S0022112091003142.

A. Cloot and G. Lebon. A nonlinear stability analysis of the Bénard–Marangoni problem. *Journal of Fluid Mechanics*, 145(1):447, August 1984. ISSN 0022-1120, 1469-7645. doi: 10.1017/S0022112084003013. URL http://www.journals.cambridge.org/abstract_S0022112084003013.

Vincent Croquette. Convective pattern dynamics at low Prandtl number: Part I. *Contemporary Physics*, 30(2):113–133, March 1989a. ISSN 0010-7514, 1366-5812. doi: 10.1080/00107518908225511. URL <http://www.tandfonline.com/doi/abs/10.1080/00107518908225511>.

Vincent Croquette. Convective pattern dynamics at low Prandtl number: Part II. *Contemporary Physics*, 30(3):153–171, May 1989b. ISSN 0010-7514, 1366-5812. doi: 10.1080/00107518908222594. URL <http://www.tandfonline.com/doi/abs/10.1080/00107518908222594>.

W. Decker, W. Pesch, and A. Weber. Spiral defect chaos in Rayleigh-Bénard convection. *Physical Review Letters*, 73(5):648–651, August 1994. ISSN 0031-9007. doi: 10.1103/PhysRevLett.73.648. URL <https://link.aps.org/doi/10.1103/PhysRevLett.73.648>.

Lifang Dong, Fucheng Liu, Shuhua Liu, Yafeng He, and Weili Fan. Observation of spiral pattern and spiral defect chaos in dielectric barrier discharge in argon/air at atmospheric pressure. *Physical Review E*, 72(4):046215, October 2005. ISSN 1539-3755, 1550-2376. doi: 10.1103/PhysRevE.72.046215. URL <https://link.aps.org/doi/10.1103/PhysRevE.72.046215>.

Y. Duguet, P. Schlatter, and D. S. Henningson. Formation of turbulent patterns near the onset of transition in plane Couette flow. *Journal of Fluid Mechanics*, 650:119–129, May 2010. ISSN 0022-1120, 1469-7645. doi: 10.1017/S0022112010000297. URL https://www.cambridge.org/core/product/identifier/S0022112010000297/type/journal_article.

Robert E. Ecke, Yuchou Hu, Ronnie Mainieri, and Guenter Ahlers. Excitation of Spirals and Chiral Symmetry Breaking in Rayleigh-Bénard Convection. *Science*, 269(5231):1704–1707, September 1995. ISSN 0036-8075, 1095-9203. doi: 10.1126/science.269.5231.1704. URL <https://www.science.org/doi/10.1126/science.269.5231.1704>.

Wiktor Eckhaus. *Studies in Non-Linear Stability Theory*, volume 6 of *Springer Tracts in Natural Philosophy*. Springer Berlin Heidelberg, Berlin, Heidelberg, 1965. ISBN 978-3-642-88319-4 978-3-642-88317-0. doi: 10.1007/978-3-642-88317-0. URL <http://link.springer.com/10.1007/978-3-642-88317-0>.

David A. Egolf, Ilarion V. Melnikov, and Eberhard Bodenschatz. Importance of Local Pattern Properties in Spiral Defect Chaos. *Physical Review Letters*, 80(15):3228–3231, April 1998. ISSN 0031-9007, 1079-7114. doi: 10.1103/PhysRevLett.80.3228. URL <https://link.aps.org/doi/10.1103/PhysRevLett.80.3228>.

David A. Egolf, Ilarion V. Melnikov, Werner Pesch, and Robert E. Ecke. Mechanisms of extensive spatiotemporal chaos in Rayleigh–Bénard convection. *Nature*, 404(6779):733–736, April 2000. ISSN

0028-0836, 1476-4687. doi: 10.1038/35008013. URL <https://www.nature.com/articles/35008013>.

T. Ellingsen and E. Palm. Stability of linear flow. *The Physics of Fluids*, 18(4):487–488, April 1975. ISSN 0031-9171. doi: 10.1063/1.861156. URL <https://pubs.aip.org/pfl/article/18/4/487/459138/Stability-of-linear-flow>.

Greg Evans and Ralph Greif. Unsteady three-dimensional mixed convection in a heated horizontal channel with applications to chemical vapor deposition. *International Journal of Heat and Mass Transfer*, 34(8):2039–2051, August 1991. ISSN 00179310. doi: 10.1016/0017-9310(91)90215-Z. URL <https://linkinghub.elsevier.com/retrieve/pii/001793109190215Z>.

Brian F. Farrell. Optimal excitation of perturbations in viscous shear flow. *The Physics of Fluids*, 31(8):2093–2102, August 1988. ISSN 0031-9171. doi: 10.1063/1.866609. URL <https://pubs.aip.org/pfl/article/31/8/2093/966463/Optimal-excitation-of-perturbations-in-viscous>.

Keisuke Fukui, Masamoto Nakajima, and Hiromasa Ueda. The longitudinal vortex and its effects on the transport processes in combined free and forced laminar convection between horizontal and inclined parallel plates. *International Journal of Heat and Mass Transfer*, 26(1):109–120, January 1983. ISSN 00179310. doi: 10.1016/S0017-9310(83)80013-1. URL <https://linkinghub.elsevier.com/retrieve/pii/S0017931083800131>.

K. S. Gage and W. H. Reid. The stability of thermally stratified plane Poiseuille flow. *Journal of Fluid Mechanics*, 33(1):21–32, July 1968. ISSN 0022-1120, 1469-7645. doi: 10.1017/S0022112068002326. URL https://www.cambridge.org/core/product/identifier/S0022112068002326/type/journal_article.

J. F. Gibson, J. Halcrow, and P. Cvitanović. Visualizing the geometry of state space in plane Couette flow. *Journal of Fluid Mechanics*, 611:107–130, September 2008. ISSN 0022-1120, 1469-7645. doi: 10.1017/S002211200800267X. URL https://www.cambridge.org/core/product/identifier/S002211200800267X/type/journal_article.

J. F. Gibson, J. Halcrow, and P. Cvitanović. Equilibrium and travelling-wave solutions of plane Couette flow. *Journal of Fluid Mechanics*, 638:243–266, November 2009. ISSN 0022-1120, 1469-7645. doi: 10.1017/S0022112009990863. URL https://www.cambridge.org/core/product/identifier/S0022112009990863/type/journal_article.

Sébastien Gomé, Laurette S. Tuckerman, and Dwight Barkley. Statistical transition to turbulence in plane channel flow. *Physical Review Fluids*, 5(8):083905, August 2020. ISSN 2469-990X. doi: 10.1103/PhysRevFluids.5.083905. URL <https://link.aps.org/doi/10.1103/PhysRevFluids.5.083905>.

Michael D. Graham and Daniel Floryan. Exact Coherent States and the Nonlinear Dynamics of Wall-Bounded Turbulent Flows. *Annual Review of Fluid Mechanics*, 53(1):227–253, January

2021. ISSN 0066-4189, 1545-4479. doi: 10.1146/annurev-fluid-051820-020223. URL <https://www.annualreviews.org/doi/10.1146/annurev-fluid-051820-020223>.

J. Halcrow, J. F. Gibson, P. Cvitanović, and D. Viswanath. Heteroclinic connections in plane Couette flow. *Journal of Fluid Mechanics*, 621:365–376, February 2009. ISSN 0022-1120, 1469-7645. doi: 10.1017/S0022112008005065. URL https://www.cambridge.org/core/product/identifier/S0022112008005065/type/journal_article.

James M. Hamilton, John Kim, and Fabian Waleffe. Regeneration mechanisms of near-wall turbulence structures. *Journal of Fluid Mechanics*, 287:317–348, March 1995. ISSN 0022-1120, 1469-7645. doi: 10.1017/S0022112095000978. URL https://www.cambridge.org/core/product/identifier/S0022112095000978/type/journal_article.

C.Q Hoard, C.R Robertson, and A Acrivos. Experiments on the cellular structure in bénard convection. *International Journal of Heat and Mass Transfer*, 13(5):849–856, May 1970. ISSN 00179310. doi: 10.1016/0017-9310(70)90130-4. URL <https://linkinghub.elsevier.com/retrieve/pii/0017931070901304>.

B. Hof, P. G. J. Lucas, and T. Mullin. Flow state multiplicity in convection. *Physics of Fluids*, 11(10):2815–2817, October 1999. ISSN 1070-6631, 1089-7666. doi: 10.1063/1.870178. URL <https://pubs.aip.org/pof/article/11/10/2815/254396/Flow-state-multiplicity-in-convection>.

M. Z. Hossain and J. M. Floryan. Drag reduction in a thermally modulated channel. *Journal of Fluid Mechanics*, 791:122–153, March 2016. ISSN 0022-1120, 1469-7645. doi: 10.1017/jfm.2016.42. URL https://www.cambridge.org/core/product/identifier/S0022112016000422/type/journal_article.

M. Z. Hossain and J. M. Floryan. On the role of surface grooves in the reduction of pressure losses in heated channels. *Physics of Fluids*, 32(8):083610, August 2020. ISSN 1070-6631, 1089-7666. doi: 10.1063/5.0018416. URL <https://pubs.aip.org/pof/article/32/8/083610/1060903/On-the-role-of-surface-grooves-in-the-reduction-of>.

M. Z. Hossain, D. Floryan, and J. M. Floryan. Drag reduction due to spatial thermal modulations. *Journal of Fluid Mechanics*, 713:398–419, December 2012. ISSN 0022-1120, 1469-7645. doi: 10.1017/jfm.2012.465. URL https://www.cambridge.org/core/product/identifier/S002211201200465X/type/journal_article.

Yuchou Hu, Robert Ecke, and Guenter Ahlers. Convection near threshold for Prandtl numbers near 1. *Physical Review E*, 48(6):4399–4413, December 1993. ISSN 1063-651X, 1095-3787. doi: 10.1103/PhysRevE.48.4399. URL <https://link.aps.org/doi/10.1103/PhysRevE.48.4399>.

Yuchou Hu, Robert Ecke, and Guenter Ahlers. Convection for Prandtl numbers near 1: Dynamics of textured patterns. *Physical Review E*, 51(4):3263–3279, April 1995. ISSN 1063-651X, 1095-3787.

doi: 10.1103/PhysRevE.51.3263. URL <https://link.aps.org/doi/10.1103/PhysRevE.51.3263>.

Yuchou Hu, Robert E. Ecke, and Guenter Ahlers. Convection under rotation for Prandtl numbers near 1: Linear stability, wave-number selection, and pattern dynamics. *Physical Review E*, 55(6): 6928–6949, June 1997. ISSN 1063-651X, 1095-3787. doi: 10.1103/PhysRevE.55.6928. URL <https://link.aps.org/doi/10.1103/PhysRevE.55.6928>.

Harold Jeffreys. Some cases of instability in fluid motion. *Proceedings of the Royal Society of London. Series A, Containing Papers of a Mathematical and Physical Character*, 118(779):195–208, March 1928. ISSN 0950-1207, 2053-9150. doi: 10.1098/rspa.1928.0045. URL <https://royalsocietypublishing.org/doi/10.1098/rspa.1928.0045>.

Klavs F. Jensen, Erik O. Einset, and Dimitrios I. Fotiadis. Flow Phenomena in Chemical Vapor Deposition of Thin Films. *Annual Review of Fluid Mechanics*, 23(1):197–232, January 1991. ISSN 0066-4189, 1545-4479. doi: 10.1146/annurev.fl.23.010191.001213. URL <https://www.annualreviews.org/doi/10.1146/annurev.fl.23.010191.001213>.

J. John Soundar Jerome, Jean-Marc Chomaz, and Patrick Huerre. Transient growth in Rayleigh-Bénard-Poiseuille/Couette convection. *Physics of Fluids*, 24(4):044103, April 2012. ISSN 1070-6631, 1089-7666. doi: 10.1063/1.4704642. URL <https://pubs.aip.org/pof/article/24/4/044103/257562/Transient-growth-in-Rayleigh-Benard-Poiseuille>.

A. Karimi, Zhi-Feng Huang, and M. R. Paul. Exploring spiral defect chaos in generalized Swift-Hohenberg models with mean flow. *Physical Review E*, 84(4):046215, October 2011. ISSN 1539-3755, 1550-2376. doi: 10.1103/PhysRevE.84.046215. URL <https://link.aps.org/doi/10.1103/PhysRevE.84.046215>.

Genta Kawahara and Shigeo Kida. Periodic motion embedded in plane Couette turbulence: regeneration cycle and burst. *Journal of Fluid Mechanics*, 449:291–300, December 2001. ISSN 0022-1120, 1469-7645. doi: 10.1017/S0022112001006243. URL https://www.cambridge.org/core/product/identifier/S0022112001006243/type/journal_article.

R.E. Kelly. The Onset and Development of Thermal Convection in Fully Developed Shear Flows. In *Advances in Applied Mechanics*, volume 31, pages 35–112. Elsevier, 1994. ISBN 978-0-12-002031-7. doi: 10.1016/S0065-2156(08)70255-2. URL <https://linkinghub.elsevier.com/retrieve/pii/S0065215608702552>.

K.J. Kennedy and A. Zebib. Combined free and forced convection between horizontal parallel planes: some case studies. *International Journal of Heat and Mass Transfer*, 26(3):471–474, March 1983. ISSN 00179310. doi: 10.1016/0017-9310(83)90052-2. URL <https://linkinghub.elsevier.com/retrieve/pii/0017931083900522>.

E.L. Koschmieder and S.G. Pallas. Heat transfer through a shallow, horizontal convecting fluid layer. *International Journal of Heat and Mass Transfer*, 17(9):991–1002, September 1974. ISSN

00179310. doi: 10.1016/0017-9310(74)90181-1. URL <https://linkinghub.elsevier.com/retrieve/pii/0017931074901811>.

P. Le Gal, A. Pocheau, and V. Croquette. Square versus Roll Pattern at Convective Threshold. *Physical Review Letters*, 54(23):2501–2504, June 1985. ISSN 0031-9007. doi: 10.1103/PhysRevLett.54.2501. URL <https://link.aps.org/doi/10.1103/PhysRevLett.54.2501>.

Jun Liu and Guenter Ahlers. Spiral-Defect Chaos in Rayleigh-Bénard Convection with Small Prandtl Numbers. *PHYSICAL REVIEW LETTERS*, 77(15), 1996.

Mary Lowe and J. P. Gollub. Pattern Selection near the Onset of Convection: The Eckhaus Instability. *Physical Review Letters*, 55(23):2575–2578, December 1985. ISSN 0031-9007. doi: 10.1103/PhysRevLett.55.2575. URL <https://link.aps.org/doi/10.1103/PhysRevLett.55.2575>.

J-M Luijkx, Jean Karl Platten, and J Cl Legros. On the existence of thermoconvective rolls, transverse to a superimposed mean Poiseuille flow. *International Journal of Heat and Mass Transfer*, 24(7):1287–1291, 1981. ISSN 0017-9310. Publisher: Elsevier.

Dong-Jun Ma, De-Jun Sun, and Xie-Yuan Yin. Multiplicity of steady states in cylindrical Rayleigh-Bénard convection. *Physical Review E*, 74(3):037302, September 2006. ISSN 1539-3755, 1550-2376. doi: 10.1103/PhysRevE.74.037302. URL <https://link.aps.org/doi/10.1103/PhysRevE.74.037302>.

Paul Manneville. Rayleigh-Bénard Convection: Thirty Years of Experimental, Theoretical, and Modeling Work. In Gerhard Höhler, Johann H. Kühn, Thomas Müller, Joachim Trümper, Andrei Ruckenstein, Peter Wölfle, Frank Steiner, Innocent Mutabazi, José Eduardo Wesfreid, and Etienne Guyon, editors, *Dynamics of Spatio-Temporal Cellular Structures*, volume 207, pages 41–65. Springer New York, New York, NY, 2006. ISBN 978-0-387-40098-3 978-0-387-25111-0. doi: 10.1007/978-0-387-25111-0_3. URL http://link.springer.com/10.1007/978-0-387-25111-0_3. Series Title: Springer Tracts in Modern Physics.

Á. Meseguer and L.N. Trefethen. Linearized pipe flow to Reynolds number 107. *Journal of Computational Physics*, 186(1):178–197, March 2003. ISSN 00219991. doi: 10.1016/S0021-9991(03)00029-9. URL <https://linkinghub.elsevier.com/retrieve/pii/S0021999103000299>.

Stephen W. Morris, Eberhard Bodenschatz, David S. Cannell, and Guenter Ahlers. Spiral defect chaos in large aspect ratio Rayleigh-Bénard convection. *Physical Review Letters*, 71(13):2026–2029, September 1993. ISSN 0031-9007. doi: 10.1103/PhysRevLett.71.2026. URL <https://link.aps.org/doi/10.1103/PhysRevLett.71.2026>.

Stephen W. Morris, Eberhard Bodenschatz, David S. Cannell, and Guenter Ahlers. The spatio-temporal structure of spiral-defect chaos. *Physica D: Nonlinear Phenomena*, 97(1-3):164–179, October 1996. ISSN 01672789. doi: 10.1016/0167-2789(96)00096-6. URL <https://linkinghub.elsevier.com/retrieve/pii/0167278996000966>.

H. W. Müller, M. Lücke, and M. Kamps. Transversal convection patterns in horizontal shear flow. *Physical Review A*, 45(6):3714–3726, March 1992. ISSN 1050-2947, 1094-1622. doi: 10.1103/PhysRevA.45.3714. URL <https://link.aps.org/doi/10.1103/PhysRevA.45.3714>.

M. Nagata. Three-dimensional finite-amplitude solutions in plane Couette flow: bifurcation from infinity. *Journal of Fluid Mechanics*, 217:519–527, August 1990. ISSN 0022-1120, 1469-7645. doi: 10.1017/S0022112090000829. URL https://www.cambridge.org/core/product/identifier/S0022112090000829/type/journal_article.

M. Nagata. Three-dimensional traveling-wave solutions in plane Couette flow. *Physical Review E*, 55(2):2023–2025, February 1997. ISSN 1063-651X, 1095-3787. doi: 10.1103/PhysRevE.55.2023. URL <https://link.aps.org/doi/10.1103/PhysRevE.55.2023>.

X. Nicolas, A. Mojtabi, and J. K. Platten. Two-dimensional numerical analysis of the Poiseuille–Bénard flow in a rectangular channel heated from below. *Physics of Fluids*, 9(2):337–348, February 1997. ISSN 1070-6631, 1089-7666. doi: 10.1063/1.869235. URL <https://pubs.aip.org/pof/article/9/2/337/259822/Two-dimensional-numerical-analysis-of-the>.

X. Nicolas, J.-M. Luijkx, and J.-K. Platten. Linear stability of mixed convection flows in horizontal rectangular channels of finite transversal extension heated from below. *International Journal of Heat and Mass Transfer*, 43(4):589–610, February 2000. ISSN 00179310. doi: 10.1016/S0017-9310(99)00099-X. URL <https://linkinghub.elsevier.com/retrieve/pii/S001793109900099X>.

Xavier Nicolas. Revue bibliographique sur les écoulements de Poiseuille–Rayleigh–Bénard : écoulements de convection mixte en conduites rectangulaires horizontales chauffées par le bas. *International Journal of Thermal Sciences*, 41(10):961–1016, October 2002. ISSN 12900729. doi: 10.1016/S1290-0729(02)01374-1. URL <https://linkinghub.elsevier.com/retrieve/pii/S1290072902013741>.

Xavier Nicolas, Shihe Xin, and Noussaiba Zoueidi. Characterisation of a Wavy Convective Instability in Poiseuille-Rayleigh-Be’nard Flows: Linear Stability Analysis and Non Linear Numerical Simulations Under Random Excitations. In *2010 14th International Heat Transfer Conference, Volume 7*, pages 203–208, Washington, DC, USA, January 2010. ASMEDC. ISBN 978-0-7918-4942-2 978-0-7918-3879-2. doi: 10.1115/IHTC14-22256. URL <https://asmedigitalcollection.asme.org/IHTC/proceedings/IHTC14/49422/203/360332>.

Xavier Nicolas, Noussaiba Zoueidi, and Shihe Xin. Influence of a white noise at channel inlet on the parallel and wavy convective instabilities of Poiseuille-Rayleigh-Bénard flows. *Physics of Fluids*, 24(8):084101, August 2012. ISSN 1070-6631, 1089-7666. doi: 10.1063/1.4737652. URL <https://pubs.aip.org/pof/article/24/8/084101/258132/Influence-of-a-white-noise-at-channel-inlet-on-the>.

William M’F. Orr. The Stability or Instability of the Steady Motions of a Perfect Liquid and of a Viscous Liquid. Part II: A Viscous Liquid. *Proceedings of the Royal Irish Academy. Section A:*

Mathematical and Physical Sciences, 27:69–138, 1907. ISSN 00358975. URL <http://www.jstor.org/stable/20490591>. Publisher: Royal Irish Academy.

Steven A. Orszag. Accurate solution of the Orr–Sommerfeld stability equation. *Journal of Fluid Mechanics*, 50(4):689–703, December 1971. ISSN 0022-1120, 1469-7645. doi: 10.1017/S0022112071002842. URL https://www.cambridge.org/core/product/identifier/S0022112071002842/type/journal_article.

S. Ostrach and Y. Kamotani. Heat Transfer Augmentation in Laminar Fully Developed Channel Flow by Means of Heating From Below. *Journal of Heat Transfer*, 97(2):220–225, May 1975. ISSN 0022-1481, 1528-8943. doi: 10.1115/1.3450344. URL <https://asmedigitalcollection.asme.org/heattransfer/article/97/2/220/416581/Heat-Transfer-Augmentation-in-Laminar-Fully>.

MT Ouazzani, Jean-Paul Caltagirone, Gilles Meyer, and Abdelkader Mojtabi. Etude numerique et expérimentale de la convection mixte entre deux plans horizontaux à températures différentes. *International journal of heat and mass transfer*, 32(2):261–269, 1989. ISSN 0017-9310. Publisher: Elsevier.

MT Ouazzani, Jean Karl Platten, and Abdelkader Mojtabi. Etude expérimentale de la convection mixte entre deux plans horizontaux à températures différentes—II. *International journal of heat and mass transfer*, 33(7):1417–1427, 1990. ISSN 0017-9310. Publisher: Elsevier.

Hervé Pabiou, Xavier Nicolas, Shihe Xin, and Sophie Mergui. Observations d'une instabilité convective apparaissant sous la forme de rouleaux sinueux dans un écoulement de Poiseuille–Rayleigh–Bénard. *Mécanique & industries*, 4(5):537–543, 2003. ISSN 1296-2139. Publisher: Elsevier.

Hervé Pabiou, Sophie Mergui, and Christine Bénard. Wavy secondary instability of longitudinal rolls in RayleighPoiseuille flows. *Journal of Fluid Mechanics*, 542(-1):175, October 2005. ISSN 0022-1120, 1469-7645. doi: 10.1017/S0022112005006154. URL http://www.journals.cambridge.org/abstract_S0022112005006154.

Chaitanya S Paranjape. Onset of turbulence in plane Poiseuille flow. 2019. Publisher: IST Austria Klosterneuburg, Austria.

Chaitanya S. Paranjape, Yohann Duguet, and Björn Hof. Oblique stripe solutions of channel flow. *Journal of Fluid Mechanics*, 897:A7, August 2020. ISSN 0022-1120, 1469-7645. doi: 10.1017/jfm.2020.322. URL https://www.cambridge.org/core/product/identifier/S0022112020003225/type/journal_article.

Chaitanya S. Paranjape, Gökhan Yalnız, Yohann Duguet, Nazmi Burak Budanur, and Björn Hof. Direct Path from Turbulence to Time-Periodic Solutions. *Physical Review Letters*, 131(3):034002, July 2023. ISSN 0031-9007, 1079-7114. doi: 10.1103/PhysRevLett.131.034002. URL <https://link.aps.org/doi/10.1103/PhysRevLett.131.034002>.

M. R. Paul, M. I. Einarsson, P. F. Fischer, and M. C. Cross. Extensive chaos in Rayleigh-Bénard convection. *Physical Review E*, 75(4):045203, April 2007. ISSN 1539-3755, 1550-2376. doi: 10.1103/PhysRevE.75.045203. URL <https://link.aps.org/doi/10.1103/PhysRevE.75.045203>.

M.R. Paul, K.-H. Chiam, M.C. Cross, P.F. Fischer, and H.S. Greenside. Pattern formation and dynamics in Rayleigh–Bénard convection: numerical simulations of experimentally realistic geometries. *Physica D: Nonlinear Phenomena*, 184(1-4):114–126, October 2003. ISSN 01672789. doi: 10.1016/S0167-2789(03)00216-1. URL <https://linkinghub.elsevier.com/retrieve/pii/S0167278903002161>.

Anne Pellew and Richard Vynne Southwell. On maintained convective motion in a fluid heated from below. *Proceedings of the Royal Society of London. Series A. Mathematical and Physical Sciences*, 176(966):312–343, November 1940. ISSN 0080-4630, 2053-9169. doi: 10.1098/rspa.1940.0092. URL <https://royalsocietypublishing.org/doi/10.1098/rspa.1940.0092>.

Sergio Pirozzoli, Matteo Bernardini, Roberto Verzicco, and Paolo Orlandi. Mixed convection in turbulent channels with unstable stratification. *Journal of Fluid Mechanics*, 821:482–516, June 2017. ISSN 0022-1120, 1469-7645. doi: 10.1017/jfm.2017.216. URL https://www.cambridge.org/core/product/identifier/S0022112017002166/type/journal_article.

Brendan B Plapp and Eberhard Bodenschatz. Core dynamics of multi-armed spirals in Rayleigh-Bénard convection. *Physica Scripta*, T67:111–116, January 1996. ISSN 0031-8949, 1402-4896. doi: 10.1088/0031-8949/1996/T67/022. URL <https://iopscience.iop.org/article/10.1088/0031-8949/1996/T67/022>.

Brendan B. Plapp, David A. Egolf, Eberhard Bodenschatz, and Werner Pesch. Dynamics and Selection of Giant Spirals in Rayleigh-Bénard Convection. *Physical Review Letters*, 81(24):5334–5337, December 1998. ISSN 0031-9007, 1079-7114. doi: 10.1103/PhysRevLett.81.5334. URL <https://link.aps.org/doi/10.1103/PhysRevLett.81.5334>.

Brendan Bryce Plapp. Spiral pattern formation in Rayleigh-Benard convection. *Ph.D. Thesis*, page 3118, December 1997. URL <https://ui.adsabs.harvard.edu/abs/1997PhDT.....105P>.

A. Prigent and O. Dauchot. "Barber pole turbulence" in large aspect ratio Taylor-Couette flow. *Physical Review Letters*, 89(1):014501, June 2002. ISSN 0031-9007, 1079-7114. doi: 10.1103/PhysRevLett.89.014501. URL <http://arxiv.org/abs/cond-mat/0009241>. arXiv:cond-mat/0009241.

Arnaud Prigent, Guillaume Grégoire, Hugues Chaté, and Olivier Dauchot. Long-wavelength modulation of turbulent shear flows. *Physica D: Nonlinear Phenomena*, 174(1-4):100–113, January 2003. ISSN 01672789. doi: 10.1016/S0167-2789(02)00685-1. URL <https://linkinghub.elsevier.com/retrieve/pii/S0167278902006851>.

Subhashis Ray and J. Srinivasan. Analysis of conjugate laminar mixed convection cooling in a shrouded array of electronic components. *International Journal of Heat and Mass Transfer*, 35

(4):815–822, April 1992. ISSN 00179310. doi: 10.1016/0017-9310(92)90249-R. URL <https://linkinghub.elsevier.com/retrieve/pii/001793109290249R>.

Lord Rayleigh. LIX. *On convection currents in a horizontal layer of fluid, when the higher temperature is on the under side.* *The London, Edinburgh, and Dublin Philosophical Magazine and Journal of Science*, 32(192):529–546, December 1916. ISSN 1941-5982, 1941-5990. doi: 10.1080/14786441608635602. URL <https://www.tandfonline.com/doi/full/10.1080/14786441608635602>.

Satish C. Reddy and Dan S. Henningson. Energy growth in viscous channel flows. *Journal of Fluid Mechanics*, 252:209–238, July 1993. ISSN 0022-1120, 1469-7645. doi: 10.1017/S0022112093003738. URL https://www.cambridge.org/core/product/identifier/S0022112093003738/type/journal_article.

Satish C. Reddy, Peter J. Schmid, and Dan S. Henningson. Pseudospectra of the Orr–Sommerfeld Operator. *SIAM Journal on Applied Mathematics*, 53(1):15–47, February 1993. ISSN 0036-1399, 1095-712X. doi: 10.1137/0153002. URL <http://pubs.siam.org/doi/10.1137/0153002>.

Florian Reetz and Tobias M. Schneider. Invariant states in inclined layer convection. Part 1. Temporal transitions along dynamical connections between invariant states. *Journal of Fluid Mechanics*, 898:A22, September 2020. ISSN 0022-1120, 1469-7645. doi: 10.1017/jfm.2020.317. URL https://www.cambridge.org/core/product/identifier/S0022112020003171/type/journal_article.

Florian Reetz, Tobias Kreilos, and Tobias M. Schneider. Exact invariant solution reveals the origin of self-organized oblique turbulent-laminar stripes. *Nature Communications*, 10(1):2277, May 2019. ISSN 2041-1723. doi: 10.1038/s41467-019-10208-x. URL <https://doi.org/10.1038/s41467-019-10208-x>.

Florian Reetz, Priya Subramanian, and Tobias M. Schneider. Invariant states in inclined layer convection. Part 2. Bifurcations and connections between branches of invariant states. *Journal of Fluid Mechanics*, 898:A23, September 2020. ISSN 0022-1120, 1469-7645. doi: 10.1017/jfm.2020.318. URL https://www.cambridge.org/core/product/identifier/S0022112020003183/type/journal_article.

Osborne Reynolds. XXIX. An experimental investigation of the circumstances which determine whether the motion of water shall be direct or sinuous, and of the law of resistance in parallel channels. *Philosophical Transactions of the Royal Society of London*, 174:935–982, December 1883. ISSN 0261-0523, 2053-9223. doi: 10.1098/rstl.1883.0029. URL <https://royalsocietypublishing.org/doi/10.1098/rstl.1883.0029>.

Osborne Reynolds. IV. On the dynamical theory of incompressible viscous fluids and the determination of the criterion. *Philosophical Transactions of the Royal Society of London. (A.)*, 186:123–164, December 1895. ISSN 0264-3820, 2053-9231. doi: 10.1098/rsta.1895.0004. URL <https://royalsocietypublishing.org/doi/10.1098/rsta.1895.0004>.

H. T. Rossby. A study of Bénard convection with and without rotation. *Journal of Fluid Mechanics*, 36(2):309–335, April 1969. ISSN 0022-1120, 1469-7645. doi: 10.1017/S0022112069001674. URL https://www.cambridge.org/core/product/identifier/S0022112069001674/type/journal_article.

Sten Rüdiger and Fred Feudel. Pattern formation in Rayleigh-Bénard convection in a cylindrical container. *Physical Review E*, 62(4):4927–4931, October 2000. ISSN 1063-651X, 1095-3787. doi: 10.1103/PhysRevE.62.4927. URL <https://link.aps.org/doi/10.1103/PhysRevE.62.4927>.

A. Scagliarini, H. Einarsson, Á. Gylfason, and F. Toschi. Law of the wall in an unstably stratified turbulent channel flow. *Journal of Fluid Mechanics*, 781:R5, October 2015. ISSN 0022-1120, 1469-7645. doi: 10.1017/jfm.2015.498. URL https://www.cambridge.org/core/product/identifier/S002211201500498X/type/journal_article.

Andrea Scagliarini, Armann Gylfason, and Federico Toschi. Heat flux scaling in turbulent Rayleigh-Bénard convection with an imposed longitudinal wind. *Physical Review E*, 89(4):043012, April 2014. ISSN 1539-3755, 1550-2376. doi: 10.1103/PhysRevE.89.043012. URL <http://arxiv.org/abs/1311.4598>. arXiv:1311.4598 [physics].

H. Schlichting. Zur Entstehung der Turbulenz bei der Plattenströmung. *Nachrichten von der Gesellschaft der Wissenschaften zu Göttingen, Mathematisch-Physikalische Klasse*, 1933:181–208, 1933. URL <http://eudml.org/doc/59420>.

Hermann Schlichting and Klaus Gersten. Onset of Turbulence (Stability Theory). In *Boundary-Layer Theory*, pages 415–496. Springer Berlin Heidelberg, Berlin, Heidelberg, 2017. ISBN 978-3-662-52917-1 978-3-662-52919-5. doi: 10.1007/978-3-662-52919-5_15. URL http://link.springer.com/10.1007/978-3-662-52919-5_15.

A. Schlüter, D. Lortz, and F. Busse. On the stability of steady finite amplitude convection. *Journal of Fluid Mechanics*, 23(01):129, September 1965. ISSN 0022-1120, 1469-7645. doi: 10.1017/S0022112065001271. URL http://www.journals.cambridge.org/abstract_S0022112065001271.

Peter J. Schmid. Nonmodal Stability Theory. *Annual Review of Fluid Mechanics*, 39(1):129–162, January 2007. ISSN 0066-4189, 1545-4479. doi: 10.1146/annurev.fluid.38.050304.092139. URL <https://www.annualreviews.org/doi/10.1146/annurev.fluid.38.050304.092139>.

Peter J. Schmid and Dan S. Henningson. *Stability and Transition in Shear Flows*, volume 142 of *Applied Mathematical Sciences*. Springer New York, New York, NY, 2001. ISBN 978-1-4612-6564-1 978-1-4613-0185-1. doi: 10.1007/978-1-4613-0185-1. URL <http://link.springer.com/10.1007/978-1-4613-0185-1>.

Rainer Schmitz, Werner Pesch, and Walter Zimmermann. Spiral-defect chaos: Swift-Hohenberg model versus Boussinesq equations. *Physical Review E*, 65(3):037302, March 2002. ISSN 1063-651X, 1095-3787. doi: 10.1103/PhysRevE.65.037302. URL <https://link.aps.org/doi/10.1103/PhysRevE.65.037302>.

Masaki Shimizu and Paul Manneville. Bifurcations to turbulence in transitional channel flow. *Physical Review Fluids*, 4(11):113903, November 2019. doi: 10.1103/PhysRevFluids.4.113903. URL <https://link.aps.org/doi/10.1103/PhysRevFluids.4.113903>. Publisher: American Physical Society.

Jennifer H. Siggers. Dynamics of target patterns in low-Prandtl-number convection. *Journal of Fluid Mechanics*, 475:357–375, January 2003. ISSN 0022-1120, 1469-7645. doi: 10.1017/S0022112002002896. URL https://www.cambridge.org/core/product/identifier/S0022112002002896/type/journal_article.

Arnold Sommerfeld. *Ein Beitrag zur hydrodynamischen Erklärung der turbulenten Flüssigkeitsbewegungen*. 1909.

Baofang Song, Dwight Barkley, Björn Hof, and Marc Avila. Speed and structure of turbulent fronts in pipe flow. *Journal of Fluid Mechanics*, 813:1045–1059, February 2017. ISSN 0022-1120, 1469-7645. doi: 10.1017/jfm.2017.14. URL https://www.cambridge.org/core/product/identifier/S0022112017000143/type/journal_article.

Herbert Brian Squire. On the stability for three-dimensional disturbances of viscous fluid flow between parallel walls. *Proceedings of the Royal Society of London. Series A, Containing Papers of a Mathematical and Physical Character*, 142(847):621–628, November 1933. ISSN 0950-1207, 2053-9150. doi: 10.1098/rspa.1933.0193. URL <https://royalsocietypublishing.org/doi/10.1098/rspa.1933.0193>.

J. Swift and P. C. Hohenberg. Hydrodynamic fluctuations at the convective instability. *Physical Review A*, 15(1):319–328, January 1977. ISSN 0556-2791. doi: 10.1103/PhysRevA.15.319. URL <https://link.aps.org/doi/10.1103/PhysRevA.15.319>.

J. J. Tao, Bruno Eckhardt, and X. M. Xiong. Extended localized structures and the onset of turbulence in channel flow. *Physical Review Fluids*, 3(1):011902, January 2018. doi: 10.1103/PhysRevFluids.3.011902. URL <https://link.aps.org/doi/10.1103/PhysRevFluids.3.011902>. Publisher: American Physical Society.

W. Tollmien. Über die Entstehung der Turbulenz. 1. Mitteilung. *Nachrichten von der Gesellschaft der Wissenschaften zu Göttingen, Mathematisch-Physikalische Klasse*, 1929:21–44, 1928. URL <http://eudml.org/doc/59276>.

Lloyd N. Trefethen. Pseudospectra of Linear Operators. *SIAM Review*, 39(3):383–406, January 1997. ISSN 0036-1445, 1095-7200. doi: 10.1137/S0036144595295284. URL <http://pubs.siam.org/doi/10.1137/S0036144595295284>.

Takahiro Tsukahara, Kaoru Iwamoto, Hiroshi Kawamura, and Tetsuaki Takeda. DNS of heat transfer in a transitional channel flow accompanied by a turbulent puff-like structure, September 2014a. URL <http://arxiv.org/abs/1406.0586>. arXiv:1406.0586 [physics].

Takahiro Tsukahara, Yasuo Kawaguchi, and Hiroshi Kawamura. An experimental study on turbulent-stripe structure in transitional channel flow, 2014b. URL <https://arxiv.org/abs/1406.1378>. Version Number: 2.

Takahiro Tsukahara, Yohji Seki, Hiroshi Kawamura, and Daisuke Tochio. DNS of turbulent channel flow at very low Reynolds numbers, September 2014c. URL <http://arxiv.org/abs/1406.0248>. arXiv:1406.0248 [physics].

Laurette S. Tuckerman and Dwight Barkley. Global Bifurcation to Traveling Waves in Axisymmetric Convection. *Physical Review Letters*, 61(4):408–411, July 1988. ISSN 0031-9007. doi: 10.1103/PhysRevLett.61.408. URL <https://link.aps.org/doi/10.1103/PhysRevLett.61.408>.

Laurette S Tuckerman and Dwight Barkley. Patterns and dynamics in transitional plane Couette flow. *Physics of Fluids*, 23(4), 2011. ISSN 1070-6631. Publisher: AIP Publishing.

Laurette S. Tuckerman, Tobias Kreilos, Hecke Schröbsdorff, Tobias M. Schneider, and John F. Gibson. Turbulent-laminar patterns in plane Poiseuille flow. *Physics of Fluids*, 26(11):114103, November 2014. ISSN 1070-6631, 1089-7666. doi: 10.1063/1.4900874. URL <https://pubs.aip.org/pof/article/26/11/114103/315350/Turbulent-laminar-patterns-in-plane-Poiseuille>.

Geoffrey K. Vallis, Douglas J. Parker, and Steven M. Tobias. A simple system for moist convection: the Rainy–Bénard model. *Journal of Fluid Mechanics*, 862:162–199, March 2019. ISSN 0022-1120, 1469-7645. doi: 10.1017/jfm.2018.954. URL https://www.cambridge.org/core/product/identifier/S0022112018009540/type/journal_article.

Milton Van Dyke and Milton Van Dyke. *An album of fluid motion*, volume 176. Parabolic Press Stanford, 1982.

D. Viswanath. Recurrent motions within plane Couette turbulence. *Journal of Fluid Mechanics*, 580:339–358, June 2007. ISSN 0022-1120, 1469-7645. doi: 10.1017/S0022112007005459. URL https://www.cambridge.org/core/product/identifier/S0022112007005459/type/journal_article.

Eduardo Vitral, Saikat Mukherjee, Perry H. Leo, Jorge Viñals, Mark R. Paul, and Zhi-Feng Huang. Spiral defect chaos in Rayleigh-Bénard convection: Asymptotic and numerical studies of azimuthal flows induced by rotating spirals. *Physical Review Fluids*, 5(9):093501, September 2020. ISSN 2469-990X. doi: 10.1103/PhysRevFluids.5.093501. URL <https://link.aps.org/doi/10.1103/PhysRevFluids.5.093501>.

Fabian Waleffe. Exact coherent structures in channel flow. *Journal of Fluid Mechanics*, 435:93–102, May 2001. ISSN 0022-1120, 1469-7645. doi: 10.1017/S0022112001004189. URL https://www.cambridge.org/core/product/identifier/S0022112001004189/type/journal_article.

Fabian Waleffe. Homotopy of exact coherent structures in plane shear flows. *Physics of Fluids*, 15(6):1517–1534, June 2003. ISSN 1070-6631, 1089-7666. doi: 10.1063/1.1566753. URL <https://pubs.aip.org/pof/article/15/6/1517/448391/Homotopy-of-exact-coherent-structures-in-plane>.

José Eduardo Wesfreid. Henri Bénard: Thermal convection and vortex shedding. *Comptes Rendus. Mécanique*, 345(7):446–466, June 2017. ISSN 1873-7234. doi: 10.1016/j.crme.2017.06.006. URL <https://comptes-rendus.academie-sciences.fr/mecanique/articles/10.1016/j.crme.2017.06.006/>.

G. E. Willis and J. W. Deardorff. The oscillatory motions of Rayleigh convection. *Journal of Fluid Mechanics*, 44(04):661, December 1970. ISSN 0022-1120, 1469-7645. doi: 10.1017/S0022112070002070. URL http://www.journals.cambridge.org/abstract_S0022112070002070.

Hao-wen Xi, J. D. Gunton, and Jorge Viñals. Spiral defect chaos in a model of Rayleigh-Bénard convection. *Physical Review Letters*, 71(13):2030–2033, September 1993. ISSN 0031-9007. doi: 10.1103/PhysRevLett.71.2030. URL <https://link.aps.org/doi/10.1103/PhysRevLett.71.2030>.

Haowen Xi and J. D. Gunton. Spatiotemporal chaos in a model of Rayleigh-Bénard convection. *Physical Review E*, 52(5):4963–4975, November 1995. ISSN 1063-651X, 1095-3787. doi: 10.1103/PhysRevE.52.4963. URL <https://link.aps.org/doi/10.1103/PhysRevE.52.4963>.

Xiangkai Xiao and Baofang Song. The growth mechanism of turbulent bands in channel flow at low Reynolds numbers. *Journal of Fluid Mechanics*, 883:R1, January 2020. ISSN 0022-1120, 1469-7645. doi: 10.1017/jfm.2019.899. URL https://www.cambridge.org/core/product/identifier/S0022112019008991/type/journal_article.

Shihe Xin, Xavier Nicolas, and Patrick Le Quéré. Stability analyses of Longitudinal Rolls of Poiseuille-Rayleigh-Bénard Flows in Air-Filled Channels of Finite Transversal Extension. *Numerical Heat Transfer, Part A: Applications*, 50(5):467–490, July 2006. ISSN 1040-7782, 1521-0634. doi: 10.1080/10407780600620079. URL <http://www.tandfonline.com/doi/abs/10.1080/10407780600620079>.

Xiangming Xiong, Jianjun Tao, Shiyi Chen, and Luca Brandt. Turbulent bands in plane-Poiseuille flow at moderate Reynolds numbers. *Physics of Fluids*, 27(4):041702, April 2015. ISSN 1070-6631, 1089-7666. doi: 10.1063/1.4917173. URL <https://pubs.aip.org/pof/article/27/4/041702/1019208/Turbulent-bands-in-plane-Poiseuille-flow-at>.